REVIEW ARTICLE

annalen der physik

Graphene

www.ann-phys.org

1D and 2D Graphdiynes: Recent Advances on the Synthesis at Interfaces and Potential Nanotechnological Applications

Zhi Chen, Concepción Molina-Jirón, Svetlana Klyatskaya, Florian Klappenberger, and Mario Ruben**

In solution-based chemistry butadiyne linkage through the homocoupling reaction of alkynes is a versatile tool for the synthesis of π-conjugated polymers, scaffolds and networks. To date this strategy was actively implemented towards chemical synthesis at interfaces. In this review paper we summarize recent advances in the syntheses of 1D wires, 2D single-layers and thin films of graphdiyne-related carbon materials at interfaces and their potential applications in nanotechnology. With a high degree of π-conjunction, uniformly distributed pores and tunable electronic properties such 2D all-carbon networks with butadiyne linkages also known as 'graphdiynes' have been successfully employed in the field-effected emission devices, solar cells, for Li ion storage and oil water separation, and as catalysis or chemical sensors.

1. Introduction

Carbon plays a special role in all known forms of life. Besides the major naturally occurring "bulk" allotropes such as diamond and graphite (sp^2-hybridized) carbon exists in a large variety of low-dimensional structures (**Figure 1**). The discovery of fullerenes,[1] carbon nanotubes,[2] and graphene[3] with their extraordinary structural, mechanical, physical, and chemical properties has revolutionized science and technology. Contrary to the sp^2 case, carbon atoms featuring exclusively sp hybridization can form only one structure – the linear allotrope carbyne.[4,5] When sp^2- and sp-hybridized carbons are combined versatile bonding schemes can be obtained, leading to novel, non-natural allotropes, most prominently represented by graphyne (GY)[6] and graphdiyne (GDY)[7–10] and their variations.

In contrast to graphene, GY and GDY are predicted to have a more complex electronic structure with directional anisotropy and non-equivalent Dirac points and an appreciable band gap within a range from 0.46 to 1.22 eV, depending on the applied methods and exchange-correlation functional.[8] Moreover, their uniform pores and chemically-active triple bonds are expected to add more chemical and physical versatility as found in graphene. Therefore, theoretical studies thave predicted interesting electronic,[14–17] optical[18] and mechanical properties[19–25] of GY and GDY for applications in hole-transporting materials,[26] transistors,[27] field emission devices,[28] battery,[16,29–33] gas separation,[34–41] desalination,[42–45] catalysis[46–49] and sensors.[50]

From the technological view point an appealing approach towards 2D all-carbon networks and scaffolds is associated with the use of templating metallic substrates. Hence, a large diversity of sources of C-precursors can be used in the synthesis of 2D sp^2-hybridized carbon networks employing high temperatures or pressure under Chemical vapor deposition (CVD) conditions.[51] However, this approach has revealed only low atomic precision producing a high number of structural defects and short-range domains. To avoid these disadvantages, organic chemists explored total-synthesis-type approaches to expand polycyclic aromatic hydrocarbons. Main materials defined as molecular models for graphene and related structures were obtained by novel synthetic bottom-up protocols. Using designed molecular precursors in combination with modern advances in molecular-resolution imaging via scanning tunneling microscopy (STM) these protocols give access to the synthesis of macrocyclic π-systems with achieved atomic accuracy and represent a unique tool for the realization of novel functional nano-architectures and networks.[52]

Through Ullmann-coupling of aromatic precursors with halogen leaving groups (such as bromo or iodo substituents) Müllen and Fasel[11,12] carried out the controlled synthesis of graphene nanoribbons (GNRs) exhibiting atomically precise width under UHV-conditions on Au(111) substrates. A careful design of a series of pre-synthesized organic precursors allowed to control the shape and chemical composition of GNRs revealing armchair graphene nanoribbons (GNRs) (**Figure 2**a), chevron-type GNRs (Figure 2b),[11] nitrogen-doped GNRs (Figure 2c)[12] and zigzag GNRs (Figure 2d,e).[13]

For long decades the rich chemistry of the acetylenic functional group has been intensively used for the preparation of medium-sized scaffolds featuring subsections of GY and GDY

Z. Chen, C. Molina-Jirón, S. Klyatskaya, M. Ruben
Institute of Nanotechnology (INT)
Karlsruhe Institute of Technology (KIT)
76344, Eggenstein-Leopoldshafen, Germany
E-mail: svetlana.klyatskaya@kit.edu; mario.ruben@kit.edu

F. Klappenberger
Physik Department E20
Technische Universität München
Garching, 85748, Germany

M. Ruben
IPCMS-CNRS
Université de Strasbourg
23 rue de Loess, 67034, Strasbourg, France

DOI: 10.1002/andp.201700056

Zhi Chen obtained his BSc and MSc degrees at department of chemistry, Nankai University in 2009 and 2012 respectively. He then joined the group of Prof. Mario Ruben at Institute of Nanotechnology, Karlsruhe Institute of Technology for his PhD study. His current research topic is syntheses and surface-confined reactions of alkynes.

Concepción Molina-Jirón: after obtaining her BSc. in Chemistry in the University of Panama, she started the MSc. in Biotechnology at the same University. While studying the MSc. she spent 4 months at the University of Manchester conducting an internship on the photosynthetic acclimation of wheat. Soon after achieving the MSc. degree she moved to Karlsruhe where she carried out a placement in the institute of functional interfaces (IFG) sponsored by the KHYS Aspirant Grant in the Karlsruhe Institute of Technology (KIT), performing studies of Platelet-biomaterial interactions. Currently, she is pursuing her PhD studies in the Institute of Nanotechnology in KIT under the supervision of Prof. Mario Ruben. Her current research comprises the synthesis, characterization and physical properties of 2D organic-based materials for their application in electronics and optoelectronics devices.

Svetlana Klyatskaya obtained her PhD in 2002 from the Institute of Chemical Kinetics and Combustion, SB RAS, Novosibirsk, Russia, under supervision of Professor S. Vasilevsky. She worked on shape-persistent macrocycles with Professor S. Höger at the University of Karlsruhe. Since 2006, she has occupied a bridging position between the supramolecular engineering of functional nanosystems and organic chemistry groups working in the field of the self-assembly of functional organic molecules at surfaces and molecular magnetism.

Florian Klappenberger obtained his PhD in 2004 from the University of Regensburg, Germany, where he studied electron transport in semiconductor diodes in intense THz fields. During his postdoctoral activities at EPF Lausanne, Switzerland and TU München he focused on the design and investigation of surface-confined functional molecular nanostructures and organic thin films. For the comprehensive physico-chemical characterization he pushed forward the STM+XS approach based on combining complementary information from scanning tunneling microscopy and X-ray spectroscopy. In 2012 he has accomplished a habilitation at the TU München and where he became group leader in 2013. Currently he is Acting Professor at the TUM Department of Physics.

Mario Ruben obtained his PhD in 1998 from the University of Jena, Germany, under supervision of Prof. D. Walther. During a DAAD post-doctoral fellowship he worked in Prof. J.-M. Lehn´s research group at the ISIS-ULP in Strasbourg, France. 2001 he moved to the Institute of Nanotechnology in Karlsruhe, where he is currently working as a group leader. In addition, he accepted in 2010 a position as professor at the Université de Strasbourg, France. Additionally, in 2013, he has become Full Professor for Molecular Materials at the Institute of Inorganic Chemistry of the KIT. His research interests involve the design, synthesis and physical characterization of functional molecules and their implementation and integration into operational nanosystems.

via solution approaches (**Scheme 1**a). Advanced synthetic protocols have been developed to prepare carbon-rich compounds by oxidative Cu-mediated[53–58] or Pd/Cu-catalyzed oxidative acetylenic coupling to generate buta-1,3-diyne-1,4-diyl fragments and Sonogashira crosscoupling reactions to form aryl-acetylenic bonds.[59] These reactions have been widely explored by organic chemists for the preparation of a variety of substructures of GY and GDY such as benzannellated dehydro[12]- and [18]-annulenes (Scheme 1b).[53,54] This enabled the monitoring of a variety of physical properties as a function of the oligomer size revealing reliable correlation of structure and properties.

Recently, the alkyne homo- and crosscoupling reactions on noble metal surfaces in UHV under soft conditions have been achieved. The pertaining C-C covalent bond formation (Scheme 1c) presents a new approach towards discrete compounds or polymeric networks with a fully conjugated backbone.[60–62]

A number of excellent reviews have been written highlighting the properties and applications of modern non-natural carbon allotropes.[10] This report is limited and focused on the recent advances on synthesis of GDY carbon allotropes at interfaces and their applications in nanotechnology directly associated to the GDY structural motif.

2. Synthesis of GDY

2.1. Interfacial Bottom-Up Construction of Graphdiyne 1D-Wires and 2D-Nanosheets Under Ultrahigh Vacuum (UHV) Conditions

Ullmann-type coupling reactions using the covalent linking of custom-designed molecular precursors rely on thermally

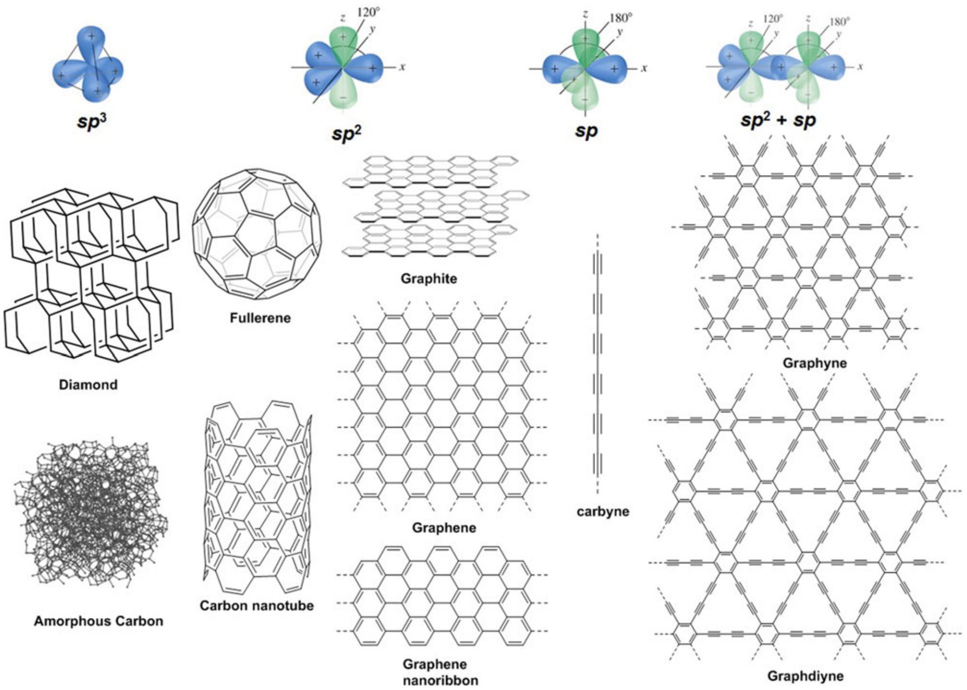

Figure 1. Variety of carbon allotropes with differently hybridized carbon.

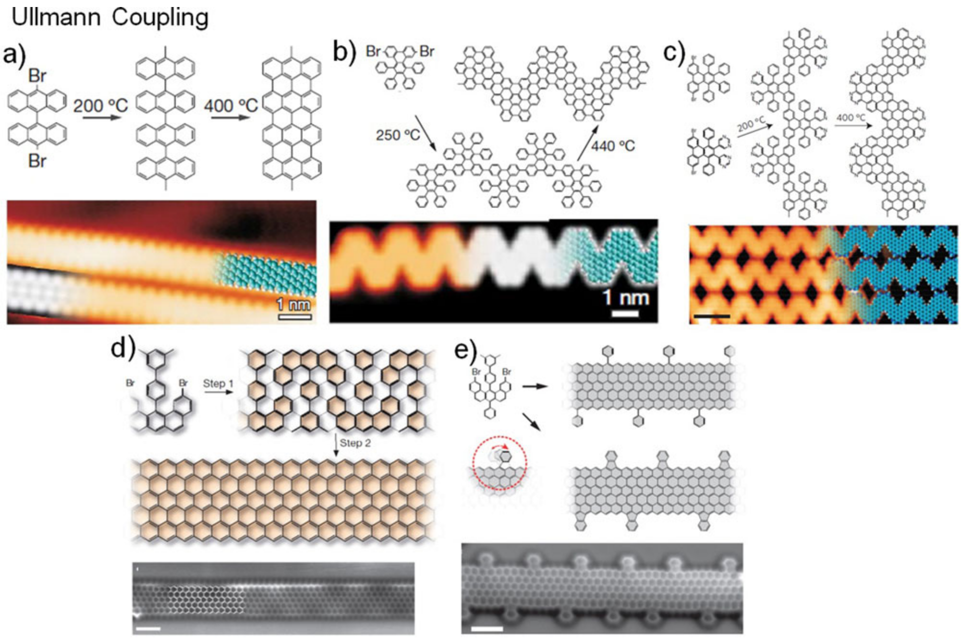

Figure 2. Chemistry-based bottom-up approaches. Ullmann-type coupling reaction schemes (up) and STM images (bottom) of $N = 7$ GNRs (a), chevron-type GNRs (b) and N-GNRs (c, scale bar, 2 nm). Reproduced with permission. (a)[11], (b)[12] Copyright 2010, 2014, Springer. Reaction schemes (up) and constant-height nc-AFM frequency-shift images (bottom) of 6-ZGNR (d, scale bar, 1 nm) and edge-modified 6-ZGNR (e, scale bar, 1 nm). Reproduced with permission.[13] Copyright 2016, Springer.

activated aryl dehalogenation followed by C-C bond formation revealing evolution of corrosive and hazardous halogens as byproducts.[11–13] In contrast, the Glaser-type homocoupling of acetylenes generates solely hydrogen as by-product (**Figure 3**a). Combined with rational precursor design, it can provide a large palette of all-carbon 2D-materials, i.e., well-defined atomic arrangements with specific bond sequences, with pores widely tunable in size and shape. Recently, we provided a deep survey on single crystal metal-surface assisted synthesis of nanoarchitectures from terminal alkynes in UHV emphasizing the differences in the coupling mechanism from solution-based reaction conditions.[55,63,64]. In the following part of the review we describe

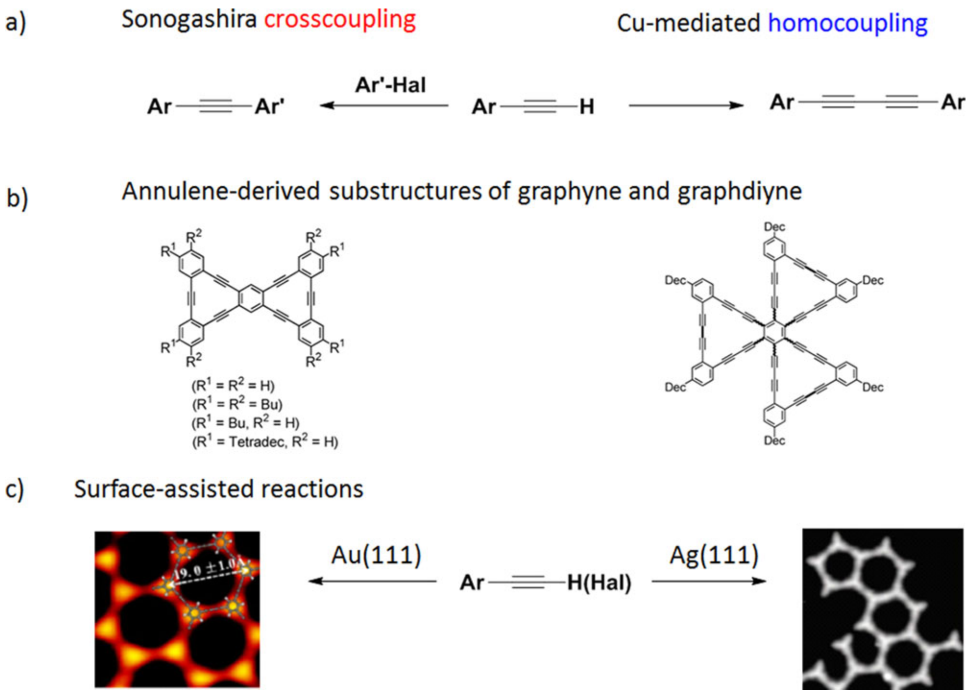

Scheme 1. Designed total-synthesis-type approaches to carbon allotropes and carbon-rich analogs based on oxidative acetylenic coupling to generate buta-1,3-diyne-1,4-diyl fragments and Sonogashira crosscoupling to form aryl-acetylenic bonds (a). (b) A series of benzannellated dehydroannulene-derived substructures of GY and GDY. Reproduced with permission.[53] Copyright 2008, De Gruyter. (c) Surface-assisted homo- and crosscoupling reactions on the noble metal surfaces in UHV. Reproduced with permission.[60,62] Copyright 2012, Springer. Copyright 2016, ACS.

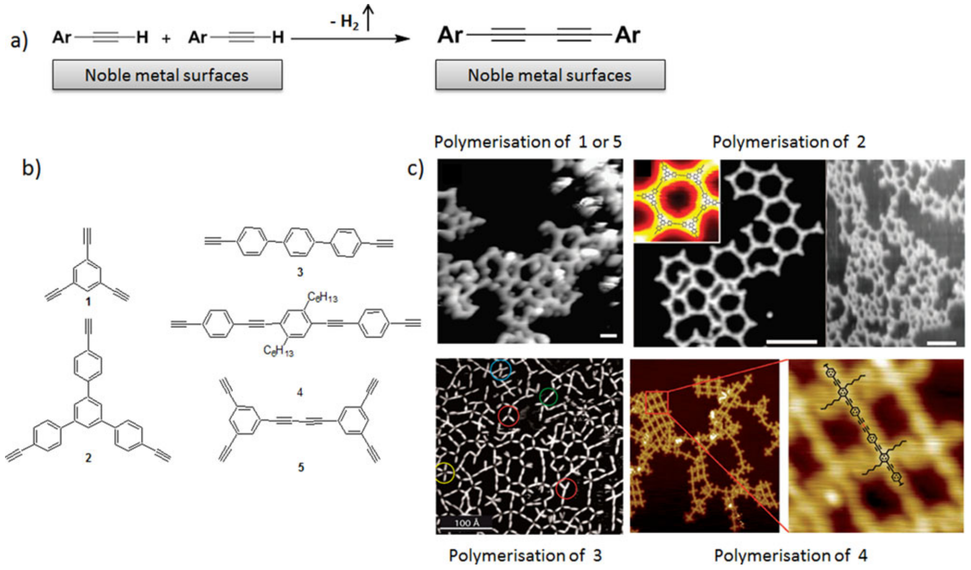

Figure 3. (a) General scheme of 2D homocoupling of acetylenes on noble metal surfaces. (b) Molecular structures of alkynes **1-5**. (c) STM images of oligomers formed from alkynes **1-5** after annealing on noble metal surfaces (Ag(111) or Au(111)). Reproduced with permission.[60, 61, 64a] Copyright 2012, Springer. Copyright 2013, Wiley. Copyright 2014, ACS.

in more details recent achievements gaining further insights in the field.

The very first example of the observation of on-surface synthesized GDY-related structures by STM was achieved in 2012, when Barth, Klappenberger and Ruben[60] deposited compounds **1** and **2** on a Ag(111) surface (Figure 3b). After annealing at 400 K, the molecules were homocoupled leading to 2D irregular, open-porous networks exhibiting locally-ordered domains with honeycomb motifs as repeating units (Figure 3c).

A reduced thermal treatment to only 300 K of the pristine organic layers formed by molecule **1** induced highly selective dimerization leading to the molecular structure **5**. However,

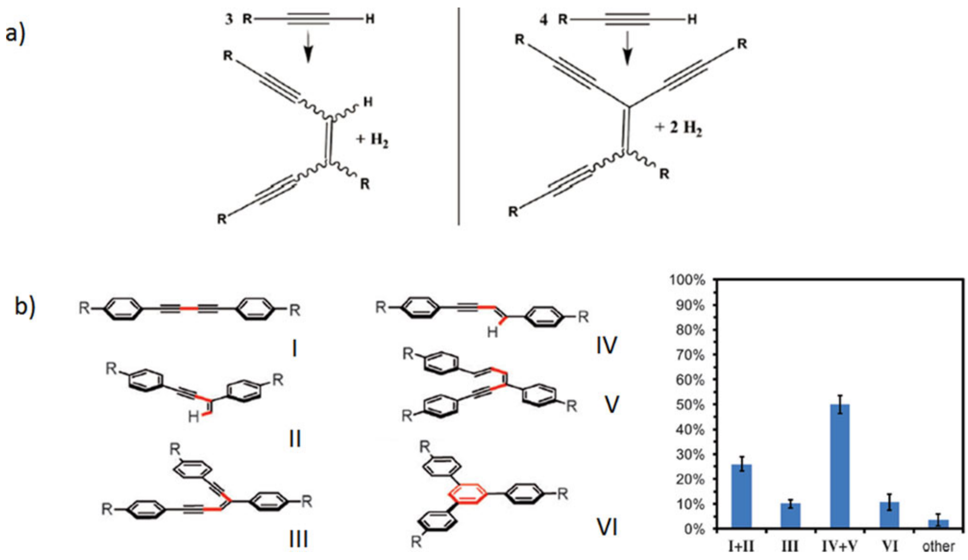

Figure 4. (a) Schematic illustrations of various side-reactions. Reproduced with permission.[60] Copyright 2012, Springer. (b) A broad range of side products resulting from polymerization of terminal alkynes. (c) Statistical analysis of the distribution of the observed products. Reproduced with permission.[61] Copyright 2013, Wiley.

upon subsequent thermal activation the interference of spurious side reactions was observed, whereby no long-range order network could be detected. Moreover, when **5** was employed as pre-synthesized monomer on Ag(111) irregular oligomerization occurred as well.[64] The analysis of the reaction products reveals formation of 2D conjugated irregular, open-porous networks similar to the one produced from compound **1**. In a similar manner, when the linear ditopic terphenylene derivate **3** was deposited on Ag(111), a hydrocarbon scaffold containing various connection motifs between up to five molecules was observed.[64]

Almost simultaneously, Fuchs et al. utilized the organic layers formed by molecules **4** featuring alkane side chains onto Au(111).[61] Analysis by means of UHV-STM unambiguously proves the oligomerization of all employed molecules via the covalent coupling of the alkyne functions: with the STM tip oligomers can be moved without destroying the connections, although also here several types of side product could be identified.

Apart from the targeted butadiyne products as a result of homo-coupling reaction, various coupling motifs resulting from covalent coupling of up to four monomers (**Figure 4**a) were observed. These revealed different side-reactions as E/Z hydrogenation, multiple insertion reactions or alkyne trimerization (Figure 4b), which provides bifurcation points with benzene core structures within the formed 2D networks (VI).

In order to overcome obvious obstacles in the fabrication of regular GDY networks and to improve the control over on surface processes several approaches have been developed, such as geometrical shielding of the butadiyne linkage or templating on vicinal surfaces[55]. Indeed, Fuchs et al[61] introduced *ortho* substituents next to the alkyne functionality resulting in 1,4-diethynyl-2,5-dihexylbenzene **6** (**Figure 5**a). Thus, bulky side groups in close proximity of the alkyne functions in combination with the Ag(111) surface lead to the selection of the linear C-C homo-coupling over other covalent coupling schemes as confirmed by the statistical analysis of the formed products. In a strategically similar approach, Wu et al.[65] demonstrated the formation of 1D covalently-bounded GDY molecular chains as the main product after annealing of 2,5-diethynyl-1,4-bis(phenylethynyl)benzene **7** (DEBPB) on the Ag(111) surface (**Figure 6**, right). The relatively high yield of ca 70% clearly confirms the effectiveness of the steric shielding by the bulky phenylethynyl-group.

Alternatively, a templating approach can achieve the formation of long polymer chains and simultanous suppression of chain branching by using the high index surfaces. Consequently, to direct C−C coupling reaction towards linear butadiyne scaffolds, Barth, Ruben and Klappenberger used the Ag(877) vicinal surface to enhance the chemoselectivity (Figure 5b).[64a] The preferential absorption sites of compound **3** were identified in the low concentration regime when molecules were evaporated onto Ag(877) substrates held at 186 K. The molecules bind preferentially to the lower step edges with their aromatic backbone parallel to latter (Figure 5b). Regular alignment close to the step-edge retains favorable even at saturation representing the ideal pre-reaction ordering. After annealing at 450 K, 1D extended-GDY wires with lengths reaching 30 nm have been obtained. The consistence and stability of newly formed bonds have been proved finally via in-situ chain manipulation through laterally displacing the STM tip. A first valuation of its electronic properties by means of DFT calculation avowed the GDY nanowires as 1D semiconductor with a presumably favorable, simple electronic band structure.[64a]

Terminal alkynes can easily react with metal atoms forming acetylides, in particular silver acetylides, which have been considered as the most powerful reactant in the transformation of alkynes.[66] Notwithstanding, there is only a limited number of reports, where formation of organometallic nanostructures at surfaces has also been achieved. Therefore, the interaction of the terminal alkynes with surface metal atoms by using 2,5-diethynyl-1,4-bis(phenylethynyl)benzene **7** on Ag (110) and Ag (100) was shown to lead to the 1D organometallic molecular

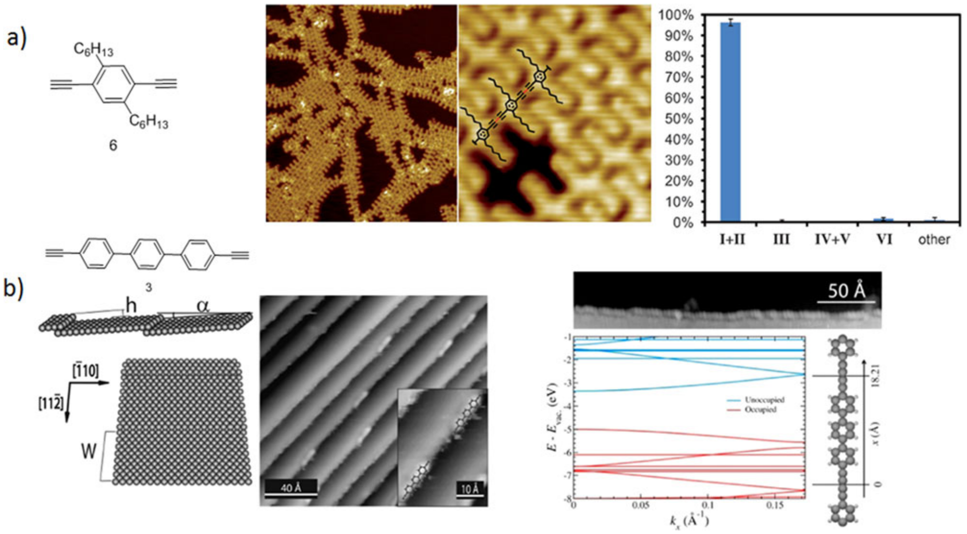

Figure 5. Steering the chemoselectivity of the alkyne homocoupling under 2D confinement (a): by steric shielding: molecular structures of alkyne and high-resolution STM image of 1,4-diethynyl-2,5-dihexylbenzene **6** on Ag(111) after 398 K annealing (0.5 V, 50 pA, 40 nm × 40 nm and 5 nm × 5 nm) and statistical analysis of the distribution of the observed products. Reproduced with permission.[61] Copyright 2013, Wiley. (b) By templating on vicinal surfaces: Molecular structures of alkyne **3**; model of the ideal Ag(877) surface with a terrace width of $W = 36.6$ Å, step height $h = 2.35$ Å and miscut angle $\alpha = 3.67°$ with respect to the (111) plane. The STM image shows the preferential step-edge absorption of individual molecules at low temperatures and the formation of extended connected structures of ca 268 Å long after annealing the sample at 450K; right: electronic band structure obtained from DG calculations. Reproduced with permission.[64a] Copyright 2014, ACS.

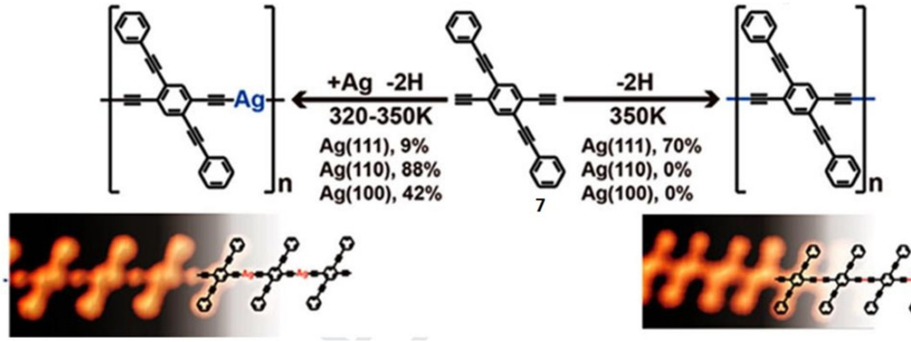

Figure 6. Different lattice planes of the Ag substrates trigger the reaction pathways and main products: homo-coupling is dominant on Ag (111), while Ag (110) triggers the formation of highly oriented 1D silver–acetylide organometallic chains. Reproduced with permission.[65] Copyright 2015, ACS.

wires with a yield of almost 90% (Figure 6, left).[65] The detailed experimental and theoretical analysis in combination with studies on Ag (111) revealed a lattice-type dependence of the terminal alkyne reaction, which originates from the epitaxial matching degree between the respective periodicities of the produced molecular wires and the underlying substrate lattices.

Organometallic bonding of molecular precursors with alkynyl functionalities represents a great opportunity for the controllable fabrication of highly-regular low-dimensional all carbon nanoscaffolds (**Figure** 7a).

Xu et al.[62] successfully explored dehalogenative homocoupling reactions of various terminal alkynyl bromides on Au (111) surface achieving the formation of dimer structures, 1D molecular nanowires and highly regular 2D molecular honeycomb networks of GDY nanostructures (Figure 7b, c). From the interplay of HR-STM imaging and DFT calculations the stepwise nature of the chemical process was unraveled. At the first step, gentle annealing reveals the formation of a large area of C-Au-C organometallic networks. Upon increasing the annealing temperature to more than 420 K, 1D molecular wires (Figure 7b) and 2D molecular network (Figure 7c) with acetylenic scaffolds evolved. Despite the formation of corrosive and hazardous halogens as byproducts during the dehalogenative homocoupling reactions, this type of on-surface transformations provides an alternative approach for fabrication of regular low-dimensional GDY-nanostructures.

2.2. Synthesis of Graphdiyne Films on Cu Foil in Solution

The bottom-up approach in combination with HR-STM molecular imaging in UHV at well-defined metal surfaces enables the investigation of chemical processes at single molecular level with deep inside into absorption geometries and chemical states of precursors, intermediates and products. Despite that, this

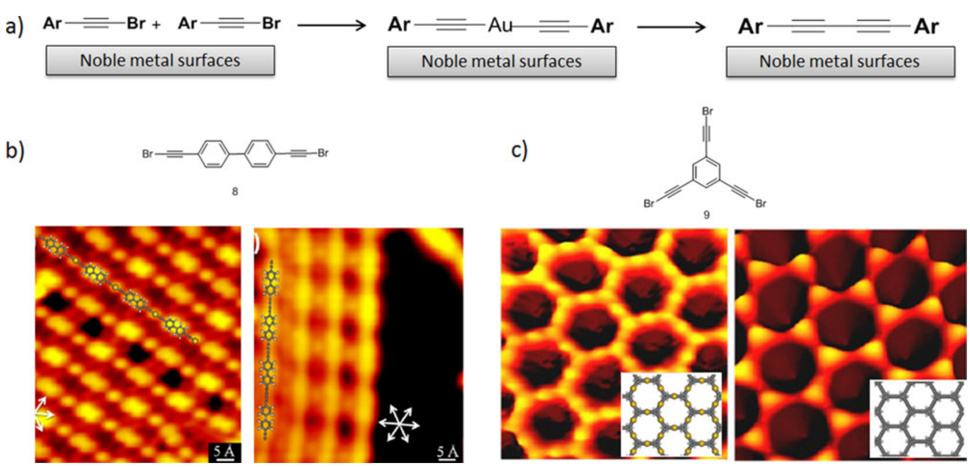

Figure 7. (a) Schematic representation of dehalogenative homocoupling reactions on Au (111) surfaces representing step-like processes with formation of C-Au-C organometallic intermediates followed by C-C homocoupling upon subsequent de-metalation. (b) Molecular structure of bBEBP **8**; STM images of organometallic chains after deposition of **8** onto Au(111) at RT and slight annealing (left) and 1D GDY-molecular wires after annealing to 425K (right). (c) Molecular structure of tBEP **9**; STM images of organometallic networks after deposition of **9** onto Au(111) at RT and slight annealing (left) and molecular network mainly with acetylenic scaffoldings after annealing to 450K (right). Reproduced with permission.[62] Copyright 2016, ACS.

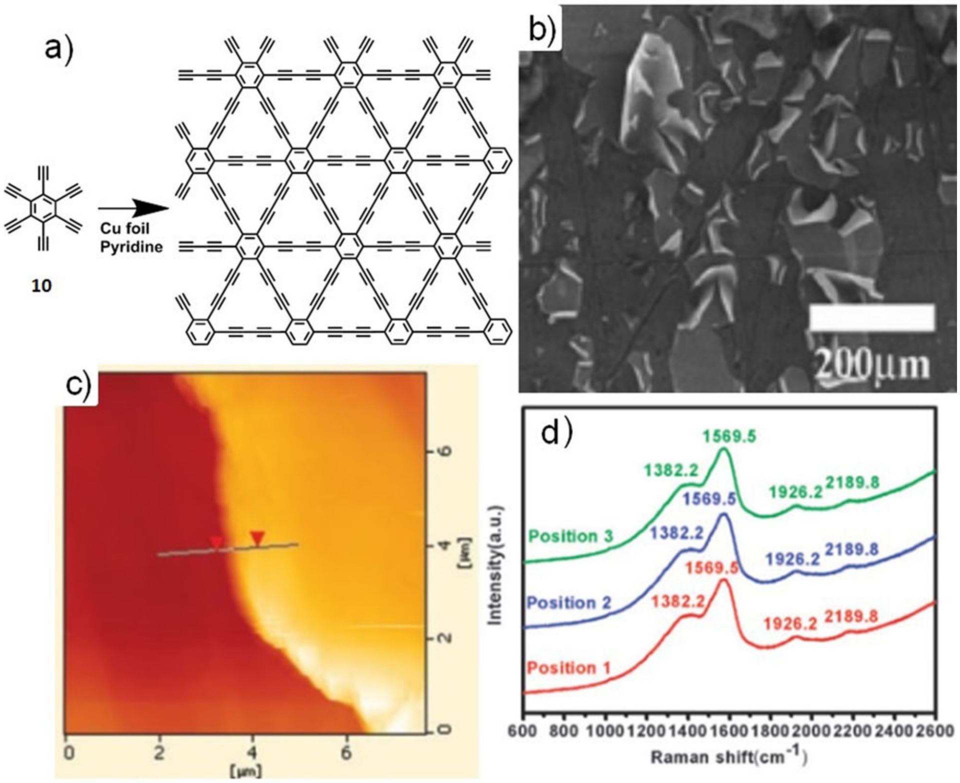

Figure 8. (a) The synthetic route of *in-situ* formation of GDY films on Cu foil. (b) SEM image of GDY films on Cu foil. (c) AFM image of GDY film (average thickness = 970 nm). (d) Raman spectra of GDY films on three different positions. Reproduced with permission.[67] Copyright 2010, RSC.

method is rather limited in terms of technological application for the production of the GDY at a big scale.

Combining the Cu salt as catalyst in solution and the metal catalyst in the UHV system, scientists tried to synthesize GDY films on Cu foil in solution in the presence of a base.

The first report of GDY synthesis on copper foil was described by Li's group in 2010, where an *in-situ* synthesis of GDY was achieved performing a cross-coupling reaction on copper foil with hexaethynylbenzene 10 (HEB) as starting material (**Figure 8**).[67]

GDY growth on copper foil was carried out in a pyridine solution, where the precursor (HEB) reacted via cross-coupling reaction for 72 h at 60 ºC under argon atmosphere. The authors obtained a very large area of GDY film (~3.6 cm^2) on copper foil

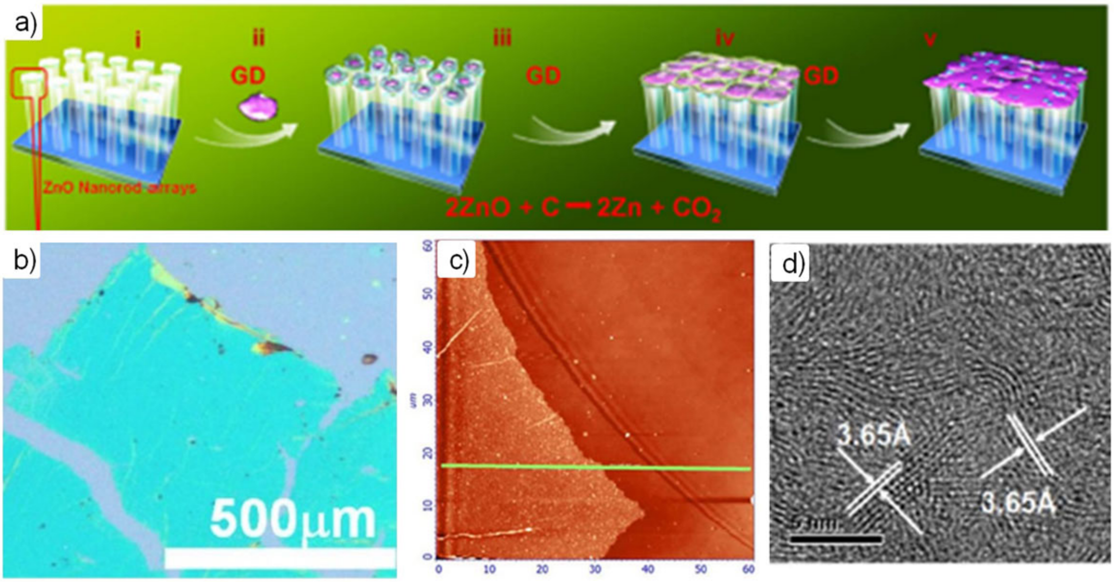

Figure 9. (a) Schematic representation of the growth of a GDY film, combining a reduction with a self-catalyzed and saturated VLS model. (b) Optical microscopy images of GDY films of 22 nm thicknesses, measured after transferring them onto SiO_2/Si substrates after dissolving the ZnO NRs. (c) AFM image of GDY films of thicknesses 22 nm. (d) HRTEM to investigate the structures of the GDY films, which show approximately distance of 0.365 nm between pairs of streaks by measurement of thicknesses of 22 nm. Reproduced with permission.[72] Copyright 2015, Springer.

support, which allowed for directional growing of GDY film due to its large flat surface area.

After transferring to a silicon substrate the film was examined and characterized employing techniques such as Raman spectroscopy, atomic force microscopy (AFM), scanning electron microscopy (SEM), and transmission electron microscopy (TEM). Figure 8b shows the SEM image of a split GDY film, where some curling in the GDY edge of the copper foil is observed signaling the flexibility of the GDY material. Further characterization was carried out employing AFM (Figure 8c), which also allows for the study of the thickness of GDY film. An average thickness of 970 nm was obtained by the authors suggesting a multilayer arrangement. High resolution transmission electron microscopy (HR-TEM) was employed to obtain images from the multilayer film, whereby the lattice fringes of 4.19 Å and the sharp spots of the selected area electron diffraction (SAED) pattern indicate a crystalline character of the atom arrangement within the film.[68]

To gain insight in the homogeneity of the film, Raman measurements were performed in different positions of the film as shown in Figure 8d, where all the spectra exhibit four main peaks at: 1382.2, 1569.5, 1926.2 and 2189.8 cm^{-1}. Via a theoretical analysis[69] the peak at 1569.5 cm^{-1} can be attributed to a C=C aromatic stretching mode of the C_6 rings similar to the G band of graphene. The peak observed at 1382.2 cm^{-1} seems to be a new D' mode differing from those in graphene as it combines the involvement of *sp*^{2} and *sp* carbon atoms. The presence of conjugated diyne links (-C≡C-C≡C-) is confirmed by the line at 2189.8 cm^{-1}. The peak at 1926.2 cm^{-1} originates from monoyne moieties and thus is a signature of remaining triple bonds not having undergone the homocoupling reaction. All modes exhibit a width much broader than in high quality graphene[70] indicating that further improvements of the structural quality are desirable for unfolding the full potential of graphdiyne.

The electrical properties of the film were probed using the Cu foil and Al films as bottom and top electrodes, respectively. The conductivity obtained was 2.5×10^{-4} S m^{-1}. Despite encouraging, further investigation of the absence of the signature of Schottky contacts, which would be expected for a metal-semiconductor interface,[71] and the origin of the required charge carriers are necessary to understand the nature of this conductivity.

Recently, Li's group[72] utilized ZnO nanorod arrays as substrate, graphdiyne powder as starting material to grow related carbon nanofilms. The precursor powder was obtained using the *in situ* cross-coupling reaction conditions (*vide supra*). The nanofilms are continuous layers, which are grown on a substrate with a nanometric scale thickness (**Figure 9**a).

In optical microscopy image a large continuous area, greater than 4.8 mm^2, could be detected exhibiting a very smooth structure (Figure 9b). Nanofilms with 22 nm thickness showed only very weak contrast with the substrate and were calculated to possess approximately 30 layers of graphdiyne (Figure 9c).

Raman spectroscopy was employed for the further characterization of the nanofilm. Of the four characteristic peaks discussed above, the ratio of the intensity of the modes related to monoyne (~1930 cm^{-1}) and diyne (~2180 cm^{-1}) moieties compared to those which can be explained by sp^2 carbon atoms (~1380 cm^{-1}, 1570 cm^{-1}) is much smaller than theoretical predictions[69] and also smaller than in the previous synthetic approach.[67] The reduction of the high-energy modes indicates that the ZnO approach is partly attacking the triple bonds. HR TEM studies moreover showed streak on the film sample with distance between streak pairs of around 0.365 nm (Figure 9d).

In order to probe the electrical properties of the such-prepared nanofilm a bottom-gate film transistor (TFT) on $OTs/SiO_2/Si$, evaporating Au electrodes directly on the GDY film transistor, was realized. The study of the electrical performance was conducted in over 100 devices yielding an average mobility of 30 cm^2 V^{-1} s^{-1}. These values are still far from the high theoretical expectations for an idealized GDY monolayer which amounts to 200000 cm^2 V^{-1} s^{-1}[73] but similar differences are known for the theoretical predictions of graphene and non-epitaxial films.

In 2015, Zhang's group[74] was able to synthetize for the first time graphdiyne nanowalls performing a modified Glaser-Hay coupling reaction (**Figure 10**a). The nanowalls can be defined as interconnected 2D nanosheets vertically standing on a substrate. The Glaser-Hay coupling reaction was performed using a copper plate instead of a copper salt and an adjusted ratio of *N,N,N',N'*-tetramethyethylenediamine (TMEDA), acetone and pyridine. As metallic copper can be easily oxidized to copper ions in presence of base, these ions act as catalyst in the reaction. The modification has improved several aspects of the original reaction such as, the very rapid rate of the coupling reaction, as a result of carrying it out in a non-alkaline solution as acetone. Improvement of the yield due to the solubility of the reagents is enhanced and small acidity of the solution bias the precursor **6** (HEB) on a positive manner, making it more stable than in the original pyridine solution. Additionally, they have shown that graphdiyne nanowalls could be grown uniformly by adapting the N-ligands quantity.

The morphology of nanowalls, obtained by SEM, exhibits a continuous matrix of vertical constructed nanowalls with large voids (Figure 10b). The cross-section suggests that the nanowalls are extraordinary uniform; around a hundred nanometers high on the whole surface. The measurements of the thickness of the nanowall films was achieved by AFM after measuring a mechanical exfoliated film transferred on a silicon surface, yielding a thickness of 15.5 nm (Figure 10c). The high crystallinity in certain areas of nanowalls films was proven by HRTEM. The value of the lattice fringe was 0.466 nm in consistence with theoretical values. Furthermore, another crystal form is present in the film suggesting curved graphdiyne sheets, evidenced by the value of the lattice parameter (0.365 nm), which is larger than that in graphene. The value of the graphdiyne nanowall is faintly larger than that of the graphene, indicating that the graphdiyne is a more delocalized system.

The Raman spectra of nanowalls displayed the four common important peaks often observed in GDY at 1383.7, 1568.7, 1939.8 and 2181.1 cm^{-1}. In this case, the triple bond related modes are much more prominent and indicate the improved structural quality of the GDY resulting from the nanowalls recipe. The field-emission performance of graphdiyne nanowalls reveals, in a typical plot of emission density J versus the applied electric field, values of E_{to} (turn-on-field) about 6.6 V μm^{-1} and a E_{thr} (threshold field) of 10.7 V μm^{-1} (Figure 10f). The value compared to vertical sheet of graphene is somewhat higher, owing to graphdiyne carrier lower mobility than in graphene. Although, the E_{to} value of graphdiyne is still considered low among of the field emission of the commonly used devices, nevertheless, in general, graphdiyne nanowalls have exhibited good field emission properties, consistent with Flowler-Nordheim (*F-N*) theory (Figure 10g), which has shown that the electron emission from nanowalls is a result of tunneling.

The use of a vapor-liquid-solid (VLS) growth process offers a series of favorable advantages to synthesize highly ordered, high-crystalline and almost defect-free nanomaterials. It offers as well a controllable approach to produce nanomaterials. This methodology has been combined with surface techniques such as coating with metals such as Au, Fe, Ni, etc., acting as catalyst.

The quest of new GDY nanostructures applicable in nanoelectronic field led to the synthesis of a different 1D form of GDY, known as GDY nanotubes (GDNT). Nanotubes are tube-like structures with nanometric scale, which in terms of aspect ratio are similar to nanowires, but unlike wires, tubes are hollow and might be single-walled or multi-walled. In this regard, Li's group[75] has performed the first attempts to fabricate GDY-based carbon tubes similar to graphene-CNTs employing an anodic aluminum oxide template, which one side was fixed to the Cu foil (**Figure 11**).

3. Applications of GDY-Materials

After the first theoretical predictions[76] GDYs have attracted now increased attention and research interest as promising materials, which can be seen from the increasing number of publications in the last decade. Thus, a set of GYs and GDYs have been not only predicted theoretically and their key properties (structural, mechanical, electronic etc.) estimated from ab initio calculations, but successfully synthesized and experimentally proved. This gives a strong impetus to further expansion of the palette of promising carbon materials and accelerates the development of modern carbon-based technologies progressing in applications of GYs and GDYs as materials for nanoelectronics, energy storage, as anode materials in batteries, as membranes for facilitating selective gas separation etc.

In this part, the experimental results and the current status and possible prospects of GDY-based nanohybrids are reviewed.

3.1. GDY-Based Nanohybrids as a Photo- and Electrocatalyst

Worldwide environmental issues, such as the treatment of waste water from the production of dye materials, textiles, and paint represent important pursuits for developing novel approaches based on the photocatalytical degradation of pollutions[77]. Inorganic semiconductor materials have been widely used in in this purpose. Among others TiO_2, ZnO, CuO, WO_3, MoO_3 etc have been extensively studied for the removal of organic contaminants due to its relative nontoxicity, low cost, and stable physical and chemical properties. However, there are several obstacles, for example, the large intrinsic bandgap of titanium oxide (3.2 eV for anatase and 3.0 eV for rutile) means that TiO_2 nanoparticles can only utilize the small ultraviolet fraction of solar light.[78] Composites with carbon-based materials like nanotube (CNT), single-walled carbon nanotubes (SWCNTs) or graphene (GR) pose enhanced photocatalytic activity.[79] These include the enhanced absorptivity of pollutants, increased light absorption intensity, increased lifetime for the electron–hole pair, and an extended light absorption range. Along this line GDY is of particular relevance due to its delocalized π systems and since their properties can be tuned along with changes in their electronic and chemical configurations (**Figure 12**a).

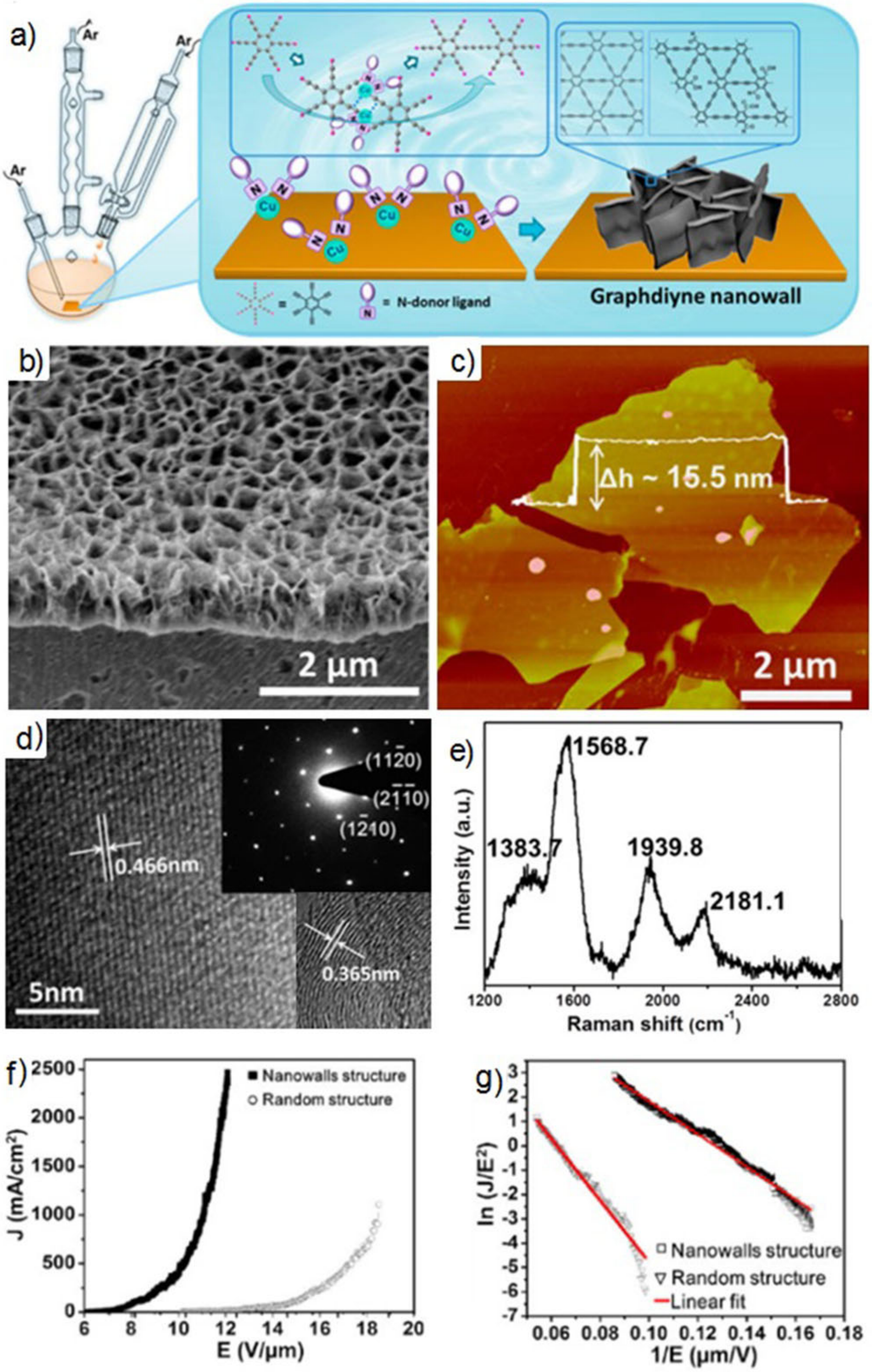

Figure 10. (a) Schematic illustration of the experimental setup. (b) Cross-sectional view of SEM image of GDY nanowalls on Cu substrate. (c) AFM image of an exfoliated sample on Si/SiO$_2$ substrate. The height profile is taken along the white line, representing a 15.5 nm thick film. (d) HR-TEM images of GDY nanowalls; SAED patterns are in corresponding insets. (e) Raman spectra of GDY nanowalls. (f) Typical plots of the electron-emission current density *J* as a function of applied electric field *E*. (g) Corresponding *F-N* plots and linear fitting. Reproduced with permission.[74] Copyright 2015, ACS.

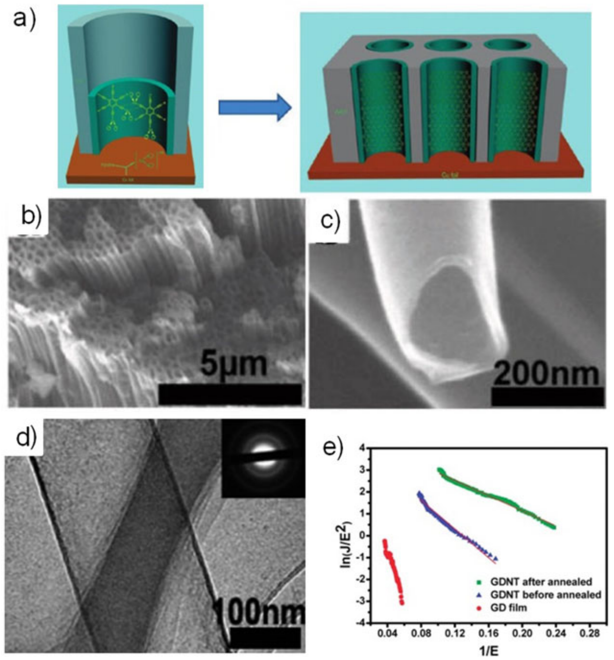

Figure 11. (a) The process and proposed mechanism to produce GDNT arrays. (b,c) The SEM images of GDNTs after being annealed. (d) High magnification TEM image of GDNTs. The inset is the corresponding SAED pattern. (e) Corresponding *F-N* plot of GDNT array before annealing (blue), after annealing (green), and GDY film (red). Reproduced with permission.[75] Copyright 2011, ACS.

Li et al.[78,83] used hydrothermal reaction to chemically bond titania nanoparticles (P25) and GDY nanosheets together, forming a novel P25-GDY nanocomposite photocatalyst. In the photocatalytic degradation of methylene blue (MB) under UV and visible light irradiation, the rate constant when using the P25-GDY composite both is better than P25, P25-CNTs and P25-GR (Figure 12b). Formation of chemical bonds between P25 and GDY effectively decreases the bandgap of P25 and extends its absorbable light range. This also is proved by the DFT calculation.[46] Such a nanocomposite photocatalyst may be a good candidate for waste water treatment.

In a similar way Venugopal's group[80] demonstrated enhanced photocatalytic activity of a GDY-ZnO nanohybrid prepared by the hydrothermal method. The rate constant of photocatalytic degradation on the both MB (Figure 12c) and rhodamine B by GDY-ZnO nanohybrids was nearly 2-fold higher compared to that of the bare ZnO nanoparticles.

Three-component complex hybrid systems of pristine GDY with Ag/AgBr using graphene oxide (GO) as a crosslinkage have been developed by Chen et al.[81] Compared to Ag/AgBr, Ag/AgBr/GO, and Ag/AgBr/GDY, the Ag/AgBr/GO/GDY exhibits an enhanced photocatalytic performance ca. 8.9, 4.3, and 2.9 times toward the degradation of methyl orange (MO) pollutant under visible light irradiation, respectively (Figure 12d). The GO not only acts as glue for hybridization GDY and Ag/AgBr nanospecies, but also performs synergistic effects with GDY sheets, promoting an efficient charge separation/transfer to enhance the catalytic performance.

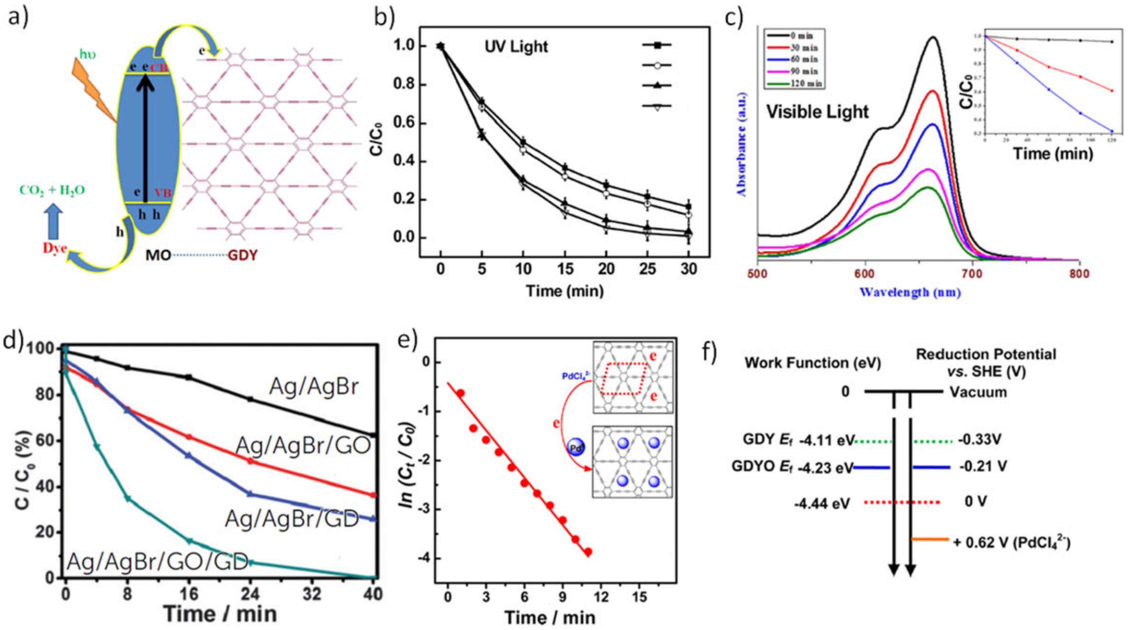

Figure 12. (a) Schematic representation of metal oxides (MO) – GDY nanohybrid photocatalysis. (b) Photocatalytic degradation of methyl blue (MB) under UV irradiation over (━■━ P25, ━○━ P25-CNTs, ━▲━ P25-GR, and ━▽━ P25-GDY). Reproduced with permission.[78] Copyright 2012, Wiley. (c) Photocatalytic performance of GD-ZnO nanohybrids over the degradation of MB measured by UV–vis spectroscopy. Rate kinetic of MB photodegradation by GDY-ZnO nanohybrids (insert, without catalyst ━■━, ZnO ━■━, ZnO-GDY━■━). Reproduced with permission[80] Copyright 2015, ACS. (d) The photodegradation of methyl orange pollutant under visible-light irradiation. Reproduced with permission.[81] Copyright 2015, RSC. (e) The catalytic reduction of 4-nitrophenol with the presence of the Pd/GDYO nanocomposite: Plot of $\ln(C_t/C_0)$ as a function of the reaction (insert, schematic illustration of formation of Pd/GDYO through electroless deposition of Pd onto GDYO). (f) Hybrid parameters: work function, and reduction potential. Reproduced with permission.[82] Copyright 2015, ACS.

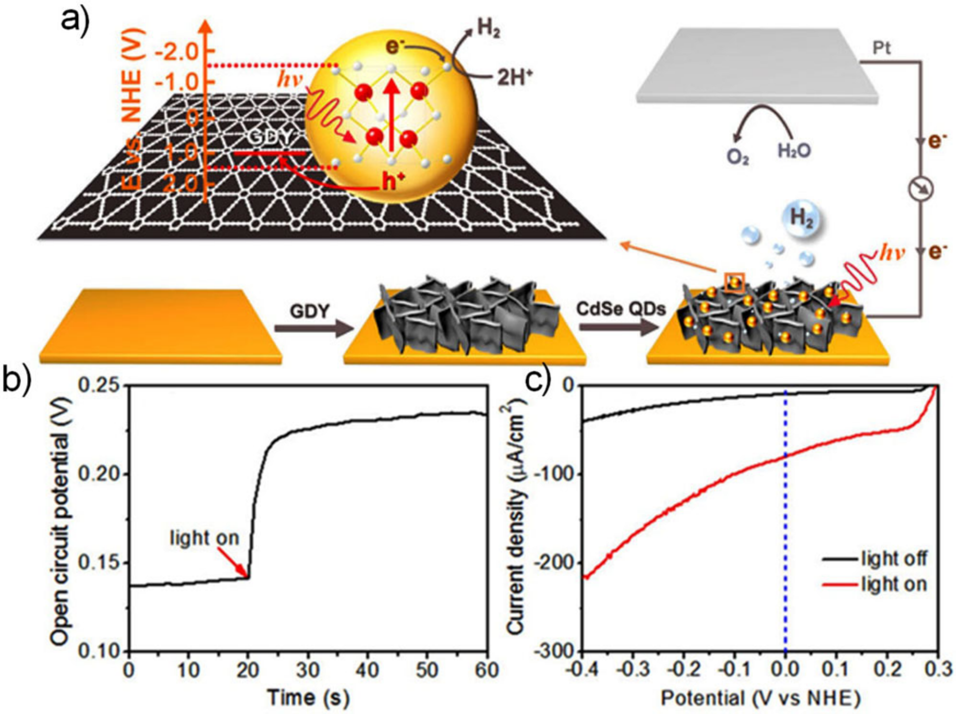

Figure 13. (a) Schematic diagram of the photoelectrochemical water splitting cell (PEC). (b) Open circuit potential response of the CdSe QDs/GDY photocathode under dark and illuminated conditions (300 W Xe lamp). (c) Linear sweep voltammetry (LSV) scanning from 0.3 to -0.4 V at 2 mV s^{-1} with light off (black trace) and on (red trace) for CdSe QDs/GDY photocathode. Reproduced with permission.[85] Copyright 2016, ACS.

GDY is also found to reduce and stabilize electroless deposition of highly dispersed Pd nanoparticles.[82] The direct reduction of $PdCl_4^{2-}$ with GDY conduced to the formation of Pd/GDYO nanocomposite with uniformly dispersed Pd nanoparticles. Combination of Pd nanoparticles distributed on the graphdiyneoxide – the oxidized form of GDY, show a more efficient catalytic performance to reduce 4-nitrophenol (4-NP) with sodium borohydride ($NaBH_4$) as a reductant as compared with those of Pd/GO, Pd/MWNT, and commercial Pd/C (**Figure 13**e).[81] On the basis of E_{cutoff} values of GDY and GDYO have been measured with ultraviolet photoelectron spectroscopy (UPS),[82] the parameters for GDY, GDYO and Pd/GDYO were also calculated. The reduction potential of GDY was estimated to be about −0.33 V vs SHE, which was lower than that of $PdCl_4{}^{2-}$ ion (+0.62 V vs SHE), suggesting its ability as the substrate for electroless deposition of Pd (Figure 13f). The reduction potential of GDY is even lower than those of other kinds of carbon allotropes such as carbon nanotubes (+0.50 V vs SHE) and graphene oxides (+0.48 V vs SCE)[84] suggesting GDY is the excellent reducing agent among all the carbon materials.

One of the most attractive topics of the modern science in the area of energy storage and environmental remediation is associated with water splitting by sunlight to produce hydrogen. GDY has been indicated recently as a promising hole transfer material to fabricate efficient photoelectrochemical water splitting cell (PEC) (Figure 13a).[85] The PEC cell constructed by Wu and Zhang consists of assembled CdSe quantum dots (QDs)/GDY photocatode and Pt wire as counter electrode. GDY nanowalls synthesized on Cu foil demonstrate high specific surface area[85], which stands for the existence of relatively strong π-π interactions between GDY and 4-mercaptopyridine surface-functionalized CdSe QDs. This leads to the beneficial hole transportation and enhancement of the photocurrent performance.

In the PEC cell test GDY, as the hole transfer layer, enhances the photocurrent performance of CdSe quantum dots (Figure 13b). The photocathode evolves H_2 with about 90% faradic efficiency within 12 h.

Replacement of the expensive Pt-based electrocatalysts currently used in fuel cells and metal–air batteries is a major prerequisite in the development of renewable energies based on the catalytical oxygen reduction reaction (ORR). In this context, graphitic carbon materials modified by N substitution, or substitutional N-doping, have been recognized as powerful catalysts for the ORR.

Zhang et al.[86] prepared the N-doped GDY (**Figure 14**a) by heating the GDY powder under high-purity ammonia mixed with Ar (10% NH_3) at 400 °C (N 400-GDY), 500 °C (N 500-GDY), 550 °C (N 550-GDY) and 600 °C (N 600-GDY), respectively.

They find that N-doped GDY, as a metal-free electro-catalyst, especially N500-GDY, has a comparable electrocatalytic activity to commercial Pt/C catalysts for ORR in alkaline fuel cells and has a better stability and an increased tolerance to the cross-over effect (Figure 14). DFT calculations show that N-doping leads to high positive charges on the carbon atoms adjacent to the N atom, which attract electrons from the anode more easily and facilitate the ORR. The N-doped GDY may be applied in fuel cell or metal-air batteries.

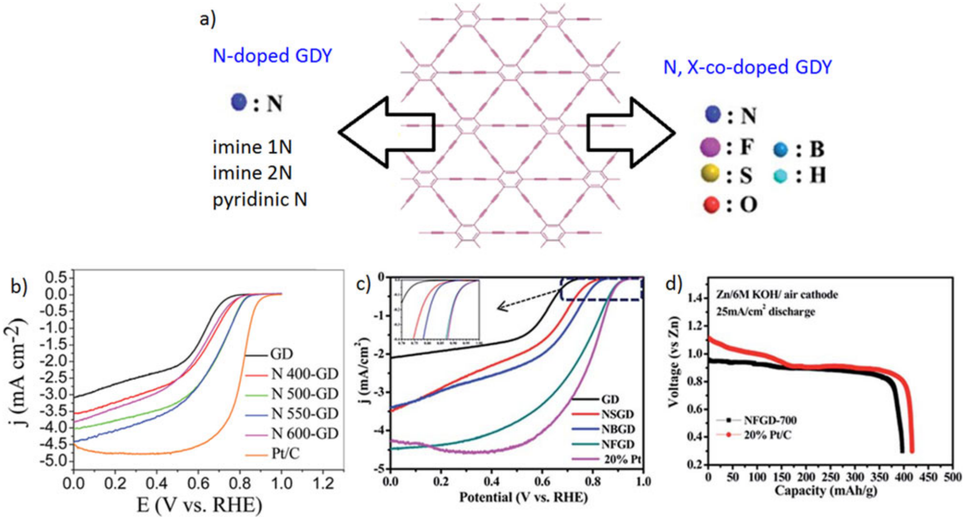

Figure 14. (a) Schematic representation of N-doped and element doped-GDY. (b) LSV curves for GDY, N-doped GDY and Pt/C on an RDE in O_2-saturated 0.1 M KOH solution at a scan rate of 10 mV s^{-1}. The rotation rate is 1600 rev min^{-1}. Reproduced with permission.[86] Copyright 2014, RSC. (c) LSV curves of GDY, NS-GDY, NB-GDY and NF-GDY obtained from rotating disk electrode (RDE) measurements at 1600 rpm at a scan rate of 10 mV s^{-1} in O_2-saturated 0.1 M KOH. (d) Typical discharge curves at 25 mA cm^{-2} of Zn-air batteries with NFGDY catalyst and 20% Pt/C as the cathode, respectively. Reproduced with permission.[87] Copyright 2016, RSC.

In 2016, the same groups[87] successfully prepared dual-heteroatom co-doped GDY: NB-GDY (N and B), NS-GDY (N and S) and NF-GDY (N and F) by 700 °C thermally treated reactions (Figure 14a). When as metal-free electrocatalyst for ORR test, the as-prepared NF-GDY exhibits comparable performance to commercial Pt/C both in half-cell (Figure 14c) and full-cell configurations (Zn-air battery) (Figure 14d), regarding its onset potential and limiting current density. It shows a much better stability as well as a higher tolerance to methanol crossover and CO poisoning effects than the commercial Pt/C. These doped GDYs have great potential for metal-free catalysts to be used as low-cost, efficient, and durable ORR catalysts.

Hijazi et al.[88] using cobalt meso-tetraethynylporphyrins as monomer *in situ* synthesized film on the multi-walled carbon nanotubes (MWNTs) surfaces through Hay coupling reaction and the multiple π-π interactions with porphyrin and MWNT (**Figure 15**a).

XPS and TEM analyses show that multilayer of Co-porphyrins form an amorphous but robust film around the nanotubes. The MWNT-CoP hybrid was tested for ORR in a series of electrochemical measurements under acidic conditions. The ORR test under acidic condition (Figure 15b) and rotating ring disk electrode (RRDE) measurements (Figure 15c) show that the MWNT-CoP have better catalytic performances of reducing oxygen into water than physisorbed monomeric systems, with an average value of transferred electrons that is close to 4.

Electrocatalytical activity of GDY-based 3D materials has been demonstrated by Yang's and Li's groups.[89] Therefore, the self-supported core-shell nanowires consisting of GDY as the shell and Cu as the core on Cu foams exhibit high cathodic catalytic activity for hydrogen evolution reaction (HER). Furthermore, catalysts comprising of GDY-cobalt nanoparticles wrapped by N-doped carbon demonstrated unprecedentedly high catalytic activity over all values of pH.

3.2. Graphdiyne for Oil Water Separation

One of the most intriguing founding in the practical application of GDY is that the morphology of graphdiyne can be readily controlled not only on 2D copper foils, as well as by 3D copper foam surface, providing great superhydrophobic materials. In this way, Zhang's group[90] produced high specific surface roughness GDY nanowalls of the ref.74 on a 3D commercially available and low-cost copper foam surface, then coated it with poly(dimethylsiloxane) (PDMS), and formed an extraordinary superhydrophobicity material (PGDCF) (with both in air (≈160.1°) and in oil (≈171.0°) (**Figure 16**a–d)).

When used for oil/water separation, it exhibits both high efficiency and good recyclability (Figure 16e). It also shows high mechanical resistance toward sandpaper abrasion cycles. This work opens a new window for GDY separation applications.

3.3. Graphdiyne for Li Ion Storage Applications

Taking into account an increasing demand for improvement of the capacity, rate performance, and life cycle of lithium-ion batteries (LIBs) the potential of GDY was further explored in the field of energy storage. There are several reports on application of GDY as high efficiency lithium storage materials and elucidate the method of lithium storage in multilayer GDY. Lithium-ion batteries featuring GDY-based electrodes exhibit excellent electrochemical performance, including high specific capacities, outstanding rate performances, and a long cycle lives.

Huang and Li's group[91] used in-situ multilayers GDY on Cu foil with scraped the GDY on one side as anode, pure Li foil as the counter electrode, formed a half cell Lithium-ion battery (**Figure 17**a). It exhibits excellent electrochemical performance, including high specific capacities, outstanding rate performances,

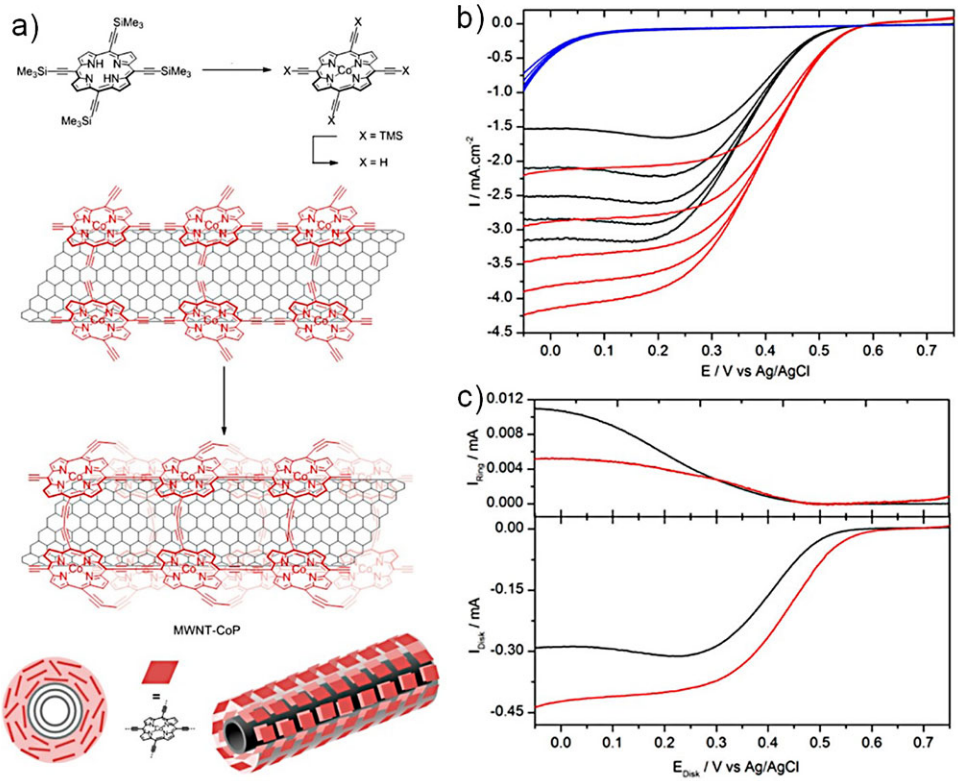

Figure 15. (a) Synthesis and representation of MWNT-CoP. (b) Polarization curves at different rotation rates (400, 800, 1200, 1600, and 2000 rpm) recorded for ORR in O_2-saturated 0.5 M H_2SO_4 solution (scan rate = 5 mV·s^{-1}, 25°C) on GC with predeposited MWNT-CoP (red), physisorbed MWNT/CoP (black), and MWNTs (blue) lines. The loading is 155 μg·cm^{-2}. (c) Rotating ring disk electrode (RRDE) measurements for MWNT-CoP (red) and physisorbed MWNT/CoP (black) (155 μg.cm^{-2}) in O_2-saturated 0.5 M H_2SO_4 (5 mV·s^{-1}, 400 rpm). The ring electrode was polarized at 1.2 V vs Ag/AgCl. Reproduced with permission.[88] Copyright 2015, ACS.

and a long cycle lives. The thicknesses also affect the electrochemical performance. Among the GDY-1 (0.24 mg cm^{-2}, thickness 10.9 μm, specific surface area 1329 m^2 g^{-1}), GDY-2 (0.48 mg cm^{-2}, 22.1 μm, 654 m^2 g^{-1}), and GDY-3 (0.72 mg cm^{-2}, 30.9 μm), the GDY-1 shows the best electrochemical performance due to the higher specific surface area and smaller thickness. It shows reversible capacities of up to 520 mA h g^{-1} after 400 cycles at a current density of 500 mA g^{-1} (Figure 17b,c). At an even higher current density of 2 A g^{-1}, cells incorporating GDY-based electrodes retained a high specific capacity of 420 mA h g^{-1} after 1000 cycles.

The same group[92] also tested the GDY powders as anode materials for lithium storage. The assembled GDY-based LIBs also exhibit excellent electrochemical performances, including a highly stable specific capacity of 552 mA h g^{-1}, for as long as 200 cycles at a current density of 50 mA g^{-1}, and outstanding rate performance. At current density of 500 mA g^{-1}, the reversible capacity is 266 mA h g^{-1}, which is less than the *in-situ* prepared GDY film on Cu foil as anode.

Furthermore, they prepared N-GDY films with NH_3 reaction on Cu foil and *in-situ* used them as electrode materials of LIBs to evaluate the properties of Li storage.[93] Compared with GDY in ref.92, the assembled batteries based on N-GDY electrode exhibit excellent electrochemical properties, containing higher reversible capacity, improved rate performance, and superior cycling stability. After 400 cycles at a current density of 500 mA g^{-1}, the batteries with a N-GDY based electrode exhibits a reversible capacity of 761 mA h g^{-1}, which is higher than 559 mA h g^{-1} for GDY.[92] The introduction of N atoms creates more heteroatomic defects and electrochemical active sites, thus enhances electrochemical performance. In addition, N-doping might be advantageous to minimize the surface side reactions and form stable interfaces, hence improving the electrochemical cycling stability of N-GDY electrodes.

Recently, the same group used bulk GDY as anode and an activated carbon (AC) as cathode to assemble a high energy and power densities Lithium-ion capacitor (LIC) (**Figure 18**a,b).[94]

This capacitor delivered an initial specific energy as high as 112.2 W h kg^{-1} at a power density of 400.1 W kg^{-1}, (about 190 Fg^{-1} at a current density of 200 mA g^{-1}) (Figure 18e), with 94.7% retention after 1000 cycles (Figure 18f). More importantly, the GDY/AC LIC showed 178 F g^{-1} of specific capacitance even at a current density as high as 500 mA g^{-1}, revealing good rate capability, with energy density of 95.1 W h kg^{-1} at a high-power density of 1000.4 W kg^{-1}. Its superior electrochemical performances may be mainly attributed to its high specific surface area due to typical 3D porous channel and its conjugated 2D atomic layer structure (Figure 18b, c).

Venugopal's group[95] also investigated the supercapacitor electrochemical properties of GDY. The GDY with carbon black and

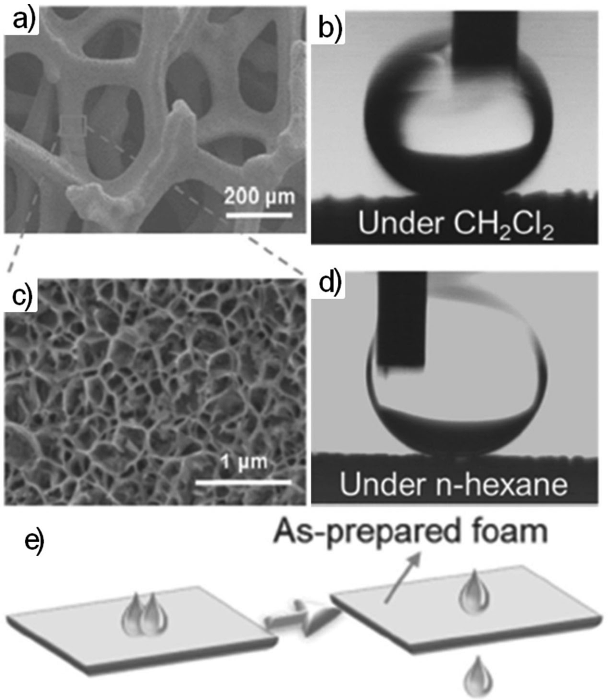

Figure 16. (a,c) Typical SEM images of the PDMS-modified GDY-grown copper foam. (b,d) The photograph of water droplet on the PGDCF surface under oil. The static contact angle (CA) water (dichloromethane) ≈ 167.2°; CA water (*n*-hexane) ≈ 171.0°. (e) Oil/water separation mechanism. Reproduced with permission.[90] Copyright 2016, Wiley.

polyvinylidenfluorid (PVDF) on stainless steel were used as working electrode, platinum as counter electrode, and Ag/AgCl as reference electrode, 1 M Na_2SO_4 solution as electrolyte (Figure 18g). The GDY electrode delivered a specific capacitance of about 71.4 F g^{-1} at a current density of 3.5 A g^{-1} (**Figure 19**h). Moreover, it had excellent capacitance retention of about 97% over 1000 cycles (Figure 18i). These results suggest that GDY have good possibility as an electrode material for supercapacitors.

3.4. Graphdiyne for Solar Cell Applications

Thanks to a physical phenomenon known as photovoltaic effect solar energy can be converted into electricity using an electronic device called "solar cell". Despite wide application in our life, there is still great demand in the improvement of their power conversion efficiency. Due to presence of both *sp*- and *sp*^{2}-hybridized carbon atoms GDY possesses natural holes, resulting in many interesting properties with clever changes in their electronic, optic, and geometric characteristics. Different groups have successfully implemented GDY in the solar cells devices, demonstrating enhanced short circuit current (J_{sc}) and power conversion efficiency (PCE).

Deng and Li's group[96] introduced GDY into poly(3-hexylthiophene) (P3HT)/[6,6]-phenyl-C61-buytyric acid methyl ester (PCBM) bulk-heterojunction solar cells. When 2.5 wt% GDY doping, it performs 56% better PCE (up to 3.52%) with enhanced J_{sc} by 2.4 mA cm^{-2} up to 10.0 mA cm^{-2} than the without doping one (Figure 19a). This improvement can be attributed to better percolation paths, and better the electron transport efficiency provided by GDY.

Meng and Li's group[97] doped GDY into P3HT hole-transporting material layer of perovskite solar cell with the device structure $FTO/TiO_2/CH_3NH_3PbI_3$/P3HT:GD/Au. As high as 14.58% PCE is achieved, better than the pristine P3HT-based solar cell (11.53%) (Figure 19b). Raman spectroscopy and ultraviolet photoelectron spectroscopy measurements show that there is relatively strong π-π stacking interaction between GDY particles and P3HT, which increases the hole transportation. On the other hand, UV-vis spectra and SAXRD show that some GDY aggregates exhibit a scattering nature, which increase the light absorption in the long wavelength range. Additionally, the devices exhibit good stability and reproducibility.

Jiu and Li's group[98] doped GDY into PCBM layer of perovskite solar cell with structure ($ITO/PEDOT:PSS/CH_3NH_3PbI_3$-xClx/PCBM:GDY/C60/Al). It increased the PCE from 13.5 to 14.8% and the J_{sc} from 22.3 to 23.4 mA cm^{-2} compared to that of pure PCBM-based ones (Figure 19c). Due to the delocalized π-systems and unique conductivity advantage, the GDY is supposed to improve the coverage of PCBM on the perovskite layer, electrical conductivity, electron mobility, and charge extraction.

Through a facile ion-beam sputtering, Ren et al.[99] deposited the Pt nanoparticles on GDY nanosheets formed a PtNP-GDNS nanocomposite. When it is used as dye-sensitized solar cells (DSSCs) counter electrodes, it improved the PCE up to 6.35% compared to 5.39% of Pt nanoparticles and 5.94% of rGO/Pt nanoparticle composites (Figure 19d). This result is also comparable with the PCE of Pt foil with PCE 7.24%. This improvement can be contributed to the special "p-n" junction-like structure with improved catalytic activity and excellent electron transfer ability after introduction of GDY.

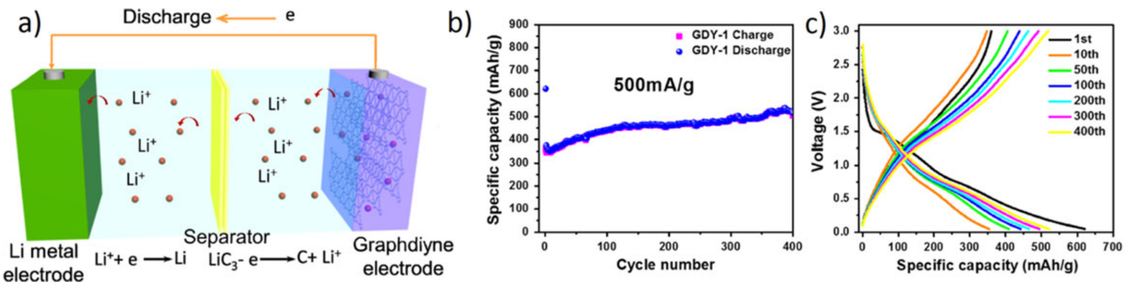

Figure 17. (a) A representation of an assembled GDY-based battery. (b) Cycle performance and (c) Galvanostatic charge/discharge profiles of the GDY-1 electrode at a current density of 2 A/g between 5 mV and 3 V in an electrolyte of 1M $LiPF_6$ in EC/DMC/DEC (1:1:1, v/v/v) containing 5% (by volume) VC. Reproduced with permission.[91] Copyright 2015, Elsevier.

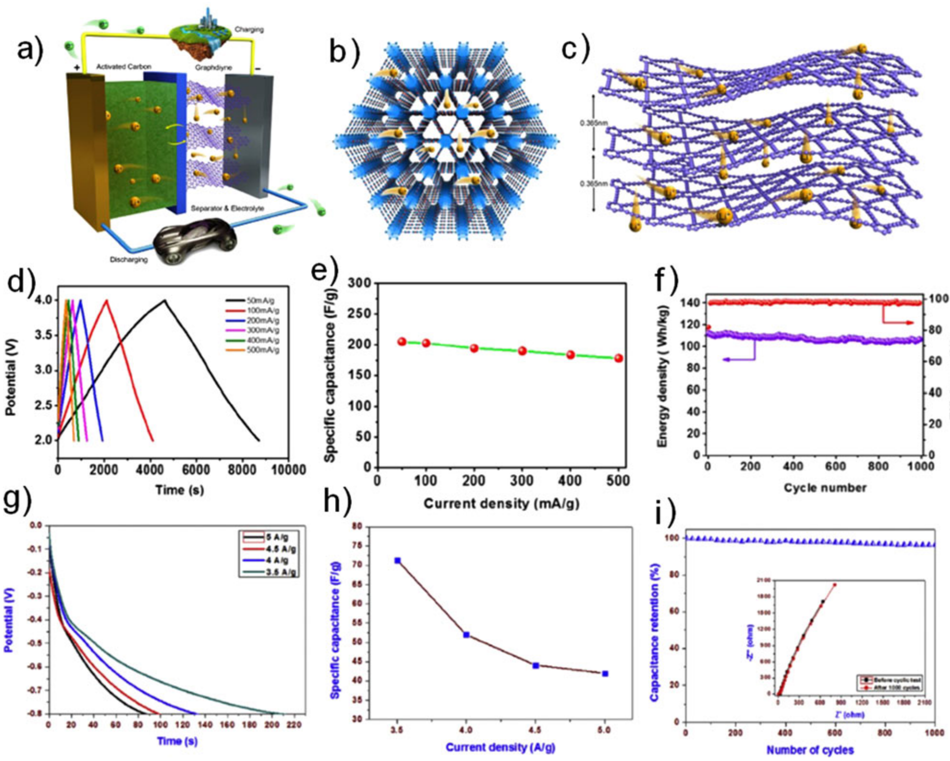

Figure 18. (a) Scheme of the GDY Li-ion capacitor. Top view (b) and side view (c) of lithium diffusion in GDY layers. (d) Galvanostatic charge-discharge voltage profiles at various current densities. (e) Corresponding specific capacitances of the LICs incorporating GDY as the negative electrode at various current densities. (f) Cycling stability of GDY/AC LIC at a current density of 200 mA g^{-1}. (g) Discharge profiles measured at different current densities (3.5-5 A g^{-1}). (h) Effect of discharge current density on the specific capacitance. (i) Capacitance retention over 1000 cycles measured using cyclic voltammetric method and the inset shows the Nyquist plot of GDY electrodes before and after cyclic tests. Reproduced with permission.[94] Copyright 2016, Elsevier.

3.5. Sensing Applications of Graphdiyne and Its Analogue

Biosensors in general are analytical devices that convert a biological response into an electrical signal. In this respect GDY owing to its high fluorescence quenching ability is used as a new platform for fluorescence sensing. The light harvesting and/or electron-conducting abilities of such a kind of nanostructures have been exploited for nanoquenching of dye-labelled and self-assembled onto the surface of nanostructures DNA via π–π stacking and/or hydrophobic interactions.

Mao's and Li's groups[100] synthesized GDY oxide using acid-treatment method and applied it as fluorescence sensor of biomolecules such as DNA and proteins (**Figure 20**a).

GDY oxide could quench the fluorescence of an organic dye (5-carboxyfluorescein (FAM)) labelled single-stranded DNA (P_{HCV}, 5'-FAM-TAA ACC CGC TCA ATG CCT GGA-3') via van der Waals force and π-π stacking interaction between nucleobases and GDY. When T_{HCV} incubated with the fluorescence quenched GDY oxide and P_{HCV} HEPES buffer solution, the fluorescence intensity increased linearly with the concentration of T_{HCV} within the concentration range from 0.017 nM to 0.4 nM. When challenged with a complementary DNA oligonucleotide, the hybridization with the complementary DNA oligonucleotide creates a double-stranded DNA (dsDNA), weakening the interactions between GDY and nucleobases and thereby liberating the dsDNA and ultimately restoring the fluorescence (Figure 20b,c). The similar fluorescence sensor behavior is also observed in FAM-labelled thrombin-binding aptamer and thrombin with GDY oxide platform. This study essentially demonstrates a new 2D nanostructure-based, robust, technically simple, high selectivity and sensitivity fluorescent sensing platform.

Wu et al.[101] used the miniemulsion-template approach and Pd(II)-Cu(I) catalyzed homocoupling of terminal alkyne groups of 5,10,15,20-tetra(4-ethynylphenyl)porphyrin-Zn(II) to synthesize the Zn-porphyrin-based conjugated microporous polymer nanoparticles (Zn-Por NCMPs) as a colorimetric sensor of SO_2 (**Figure 21**a,b).

As the Zn-Por NCMPs is of green color, after exposed to SO_2, the Zn-Por NCMPs release pyrrodidine from the metal site and turn into red (Figure 21c). This noncovalent displacement reaction is reproducible and reliable. The Zn-Por NCMPs were also coated on the test paper for rapid gas-solid interfacial detection. Using UV-vis spectroscopy, the broad peak at around 440 nm shows almost a linear decrease with stepwise added SO_2 solution. Thus the Zn-Por NCMPs material seems likely to quantitatively determine the concentration of SO_2, from μM to 0.5 mM levels.

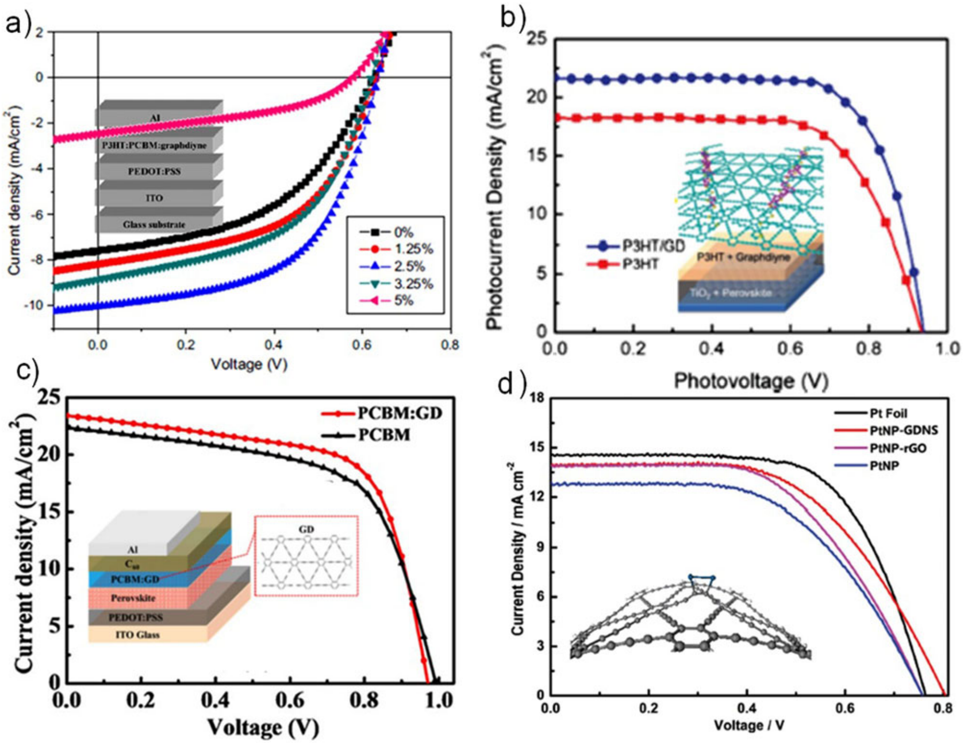

Figure 19. (a) Current-voltage (*J-V*) curves of P3HT:PCBM:GDY-based PSCs with different GDY contents (0%, 1.25%, 2.5%, 3.25%, and 5%) under 100 mW cm^{-2} AM1.5 solar simulator illumination. Inset shows the structure of photovoltaic device. Reproduced with permission.[96] Copyright 2011, Elsevier. (b) *J-V* characteristics of perovskite solar cells with different HTM layers. Inset is schematic diagram of the perovskite solar cells with P3HT hole-transporting material modified with GDY. Reproduced with permission.[97] Copyright 2015, Wiley. (c) *J-V* characteristic curves of pure PCBM and PCBM:GDY based perovskite solar cells under AM 1.5G 100 mW cm^{-2} simulated solar light. Inset shows device architecture of perovskite solar cell and chemical structure of GDY. From the bottom: ITO/PEDOT:PSS/Perovskite/PCBM:GDY/C_{60}/Al. Reproduced with permission.[98] Copyright 2015, Wiley. (d) Photocurrent density-voltage (*J-V*) curves of DSSCs using different counter electrodes. Inset is the Pt_2-GDY fragment (off-center adsorption site). Reproduced with permission.[99] Copyright 2015, ACS.

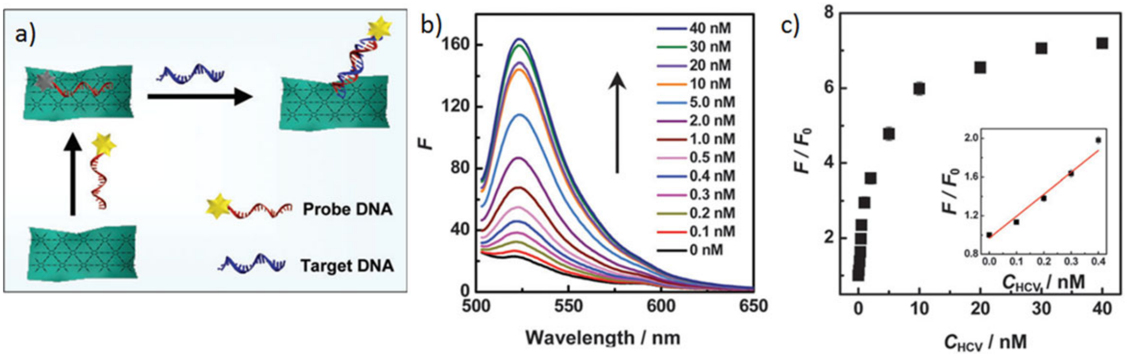

Figure 20. (a) Schematic illustration of the GDY-based fluorometric DNA assay. (b) Fluorescence spectra of P_{HCV} (20 nM) containing GDY oxide (10 μg mL^{-1}) in HEPES buffer upon incubation with T_{HCV} with different final concentrations (from bottom to top: 0.0, 0.1, 0.2, 0.3, 0.4, 0.5, 1.0, 2.0, 5.0, 10, 20, 30, and 40 nM). (c) Plot of F/F_0 versus the concentration of T_{HCV}. The inset shows the calibration curve. F_0 and F denote the intensities of the mixture of P_{HCV} (20 nM) and GD oxide (10 mg mL^{-1}) before and after incubation of P_{HCV} with T_{HCV}, respectively. Excitation wavelength, 490 nm. Emission wavelength, 523 nm. Reproduced with permission.[100] Copyright 2016, RSC.

Conclusion

In this review, the syntheses and applications of combined *sp* and sp^2 hybridized carbon allotropes of GDYs and its modifications were discussed. The morphology of GDYs synthesized can be tuned by different synthetic methods, ranging from 1D nanowires or 1D nanotubes to 2D nanofilms, 2D nanowalls and 3D sponges. Although structurally more difficult to control as the respective graphene analogues, the intriguing properties of GDYs such as, natural band gap, uniform pores and chemically-active triple bonds have been tested in various fields such as catalysis, Li ion storage, solar cells, oil water separation, and sensor applications. Moreover, GDY can form composite materials with TiO_2, ZnO, Pd and CdSe, contributing greatly to raising their

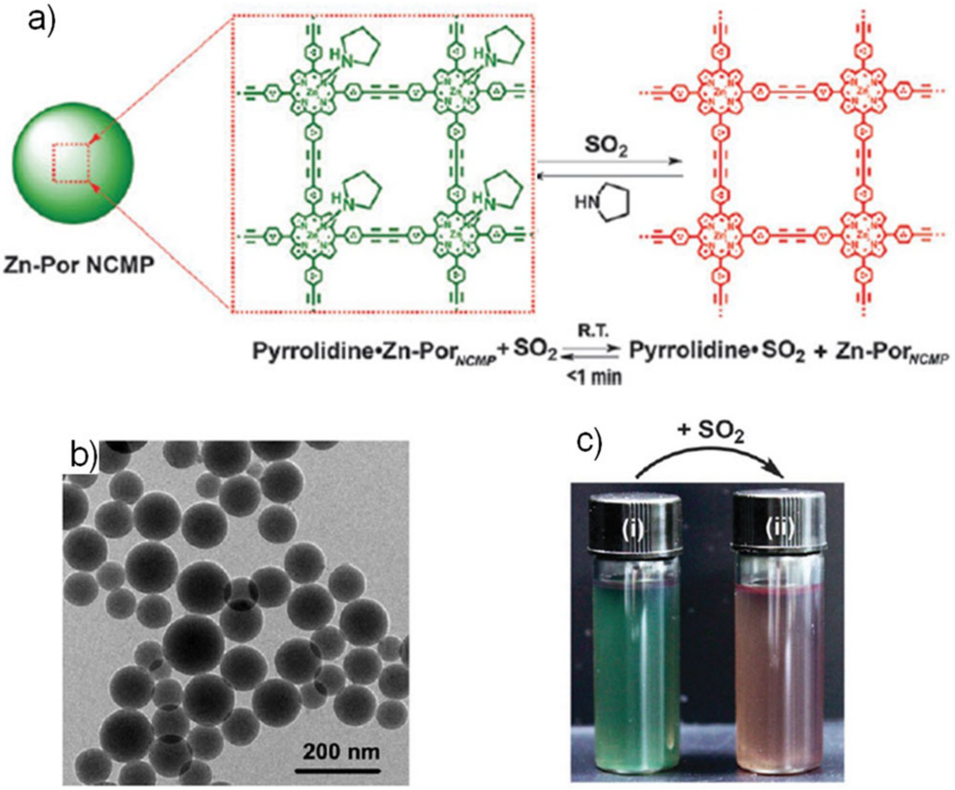

Figure 21. (a) Schematic representation of miniemulsion-mediated synthesis of Zn-Por CMP nanoparticles and their use in colorimetric detection of gaseous SO_2 via a noncovalent displacement reaction. (b) TEM image hydrodynamic diameter histogram in $CHCl_3$. (c) Visual detection showing the color change from green to red before (i) and after (ii) bubbling of SO_2 into Zn-Por NCMP solution in the presence of pyrrolidine. Reproduced with permission.[101] Copyright 2014, RSC.

properties such as photocatalyst or electocatalysis for water splitting and O_2 reduction. GDYs also show very high capacities and long-time cycle performance in Li ion battery and improve the polymer and perovskite solar cell performance.

Besides the synthesis of GDY film on Cu foil or Cu-foam in solution, the syntheses of atomically precise, flat 1D GDY wires and 2D single layer GDY analogues have been successfully realized via bottom-up approach on a single crystal metal surface in UHV condition. Though the chemoselectivity of the homocoupling reaction on planar metal surfaces is limited by various side-reactions. The implementation of steric hindrance, organometallic intermediates, or using the surface templating strategy have been proven to be powerful tools for recovering the chemoselectivity of homocoupling reaction.

Despite great efforts the synthesis of large areas of highly ordered single-layer GDYs exhibiting high crystallinity and few defects is still a big challenge. However, since GDYs represent an important novel class of 2D carbon materials with a multitude of appealing properties, this challenge will certainly be overcome in near future addressing a lot of novel interesting materials properties.

Acknowledgements

We would like to thank for the support by the DFG-priority program SPP1459: Graphene and China Scholarship Council (CSC). We acknowledge the KNMF facility (KIT, Germany) for the allocation of technical equipment.

Conflict of Interest

The authors have declared no conflict of interest.

Keywords

graphdiyne, synthesis, allotropes, applications, nanowires, thin films, interfaces

Received: January 30, 2017
Revised: April 10, 2017
Published online: July 29, 2017

---

[1] H. W. Kroto, J. R. Heath, S. C. O'Brien, R. F. Curl, and R. E. Smalley, *Nature* **318** (1985).
[2] S. Iijima, *Nature* **354**, 56–58 (1991).
[3] K. S. Novoselov, A. K. Geim, S. V. Morozov, D. Jiang, Y. Zhang, S. V. Dubonos, I. V. Grigorieva, and A. A. Firsov, *Science* **306**, 666–669 (2004).
[4] G. H. Hoorn, *Recueil des Travaux Chimiques des Pays-Bas* **7**, 341–341 (2010).

[5] L. Shi, P. Rohringer, K. Suenaga, Y. Niimi, J. Kotakoski, J. C. Meyer, H. Peterlik, M.; Wanko, S. Cahangirov, A. Rubio, Z. J. Lapin, L.; Novotny, P. Ayala, and T. Pichler, *Nat. Mater.* **15**, 634–639 (2016).
[6] R. H. Baughman, H. Eckhardt, and M. Kertesz, *J. Chem. Phys.* **87**, 6687 (1987).
[7] M. M. Haley, S. C. Brand, and J. J. Pak, *Angew. Chem., Int. Ed. Engl.* **36**, 836–838 (1997).
[8] A. L. Ivanovskii, *Prog. Solid State Chem.* **41**, 1–19 (2013).
[9] Q. Peng, A. K. Dearden, J. Crean, L. Han, S. Liu, X. Wen, and S. De, *Nanotechnol. Sci. Appl.* **7**, 1–29 (2014).
[10] Y. Li, L. Xu, H. Liu, and Y. Li, *Chem. Soc. Rev.* **43**, 2572–2586 (2014). b) M. M. Haley, *Pure Appl. Chem.*, **80**, 519–532, (2008). c) Q. Peng, A. K. Dearden, J. Crean, L. Han, S. Liu, X. Wen, and S. De, *Nanotechnology, Science and Applications*, **7**, 1–29 (2014). d) N. J. Coville, S.D. Mhlanga, E. N. Nxumalo, and A. Shaikjee, *S. Afr. J. Sci.* **107**, 418, (2011).
[11] J. Cai, P. Ruffieux, R. Jaafar, M. Bieri, T. Braun, S. Blankenburg, M. Muoth, A. P. Seitsonen, M. Saleh, X. Feng, K. Mullen, and R. Fasel, *Nature* **466**, 470–473 (2010).
[12] J. Cai, C. A. Pignedoli, L. Talirz, P. Ruffieux, H. Sode, L. Liang, V. Meunier, R. Berger, R. Li, X. Feng, K. Mullen, R. Fasel, *Nat. Nanotechnol.* **9**, 896–900 (2014).
[13] P. Ruffieux, S. Wang, B. Yang, C. Sanchez-Sanchez, J. Liu, T. Dienel, L. Talirz, P. Shinde, C. A. Pignedoli, D. Passerone, T. Dumslaff, X. Feng, K. Mullen, and R. Fasel, *Nature* **531**, 489–492 (2016).
[14] G. Luo, X. Qian, H. Liu, R. Qin, J. Zhou, L. Li, Z. Gao, E. Wang, W.-N. Mei, J. Lu, Y. Li, and S. Nagase, *Phys. Rev. B* **84**, 075439 (2011).
[15] M. Long, L. Tang, D. Wang, Y. Li, and Z. Shuai, *ACS Nano* **5**, 2593–2600 (2011).
[16] K. Srinivasu and S. K. Ghosh, *J. Phys. Chem. C* **116**, 5951–5956 (2012).
[17] J. Kang, J. Li, F. Wu, S.-S. Li, and J.-B. Xia, *J. Phys. Chem. C* **115**, 20466–20470 (2011).
[18] J. Wang, S. Zhang, J. Zhou, R. Liu, R. Du, H. Xu, Z. Liu, J. Zhang, and Z. Liu, *Phys. Chem. Chem. Phys.* **16**, 11303–11309 (2014).
[19] Y. Pei, *Physica B: Condensed Matter* **407**, 4436–4439 (2012).
[20] D. B. Brommer and M. J. Buehler, *Journal of Applied Mechanics* **80**, 040908 (2013).
[21] Y. Yang and X. Xu, *Comput. Mater. Sci.* **61**, 83–88 (2012).
[22] S. W. Cranford, D. B. Brommer, and M. J. Buehler, *Nanoscale* **4**, 7797–7809 (2012).
[23] Q. Yue, S. Chang, J. Kang, S. Qin, and J. Li, *J. Phys. Chem. C* **117**, 14804–14811 (2013).
[24] M. Becton, L. Zhang, and X. Wang, *Phys. Chem. Chem. Phys.* **16**, 18233–18240 (2014).
[25] R. E. Roman and S. W. Cranford, *Adv. Eng. Mater.* **16**, 862–871 (2014).
[26] S. Jalili, F. Houshmand, and J. Schofield, *Applied Physics A*, **119**, 571–579 (2015).
[27] Y. Pan, Y. Wang, L.; Wang, H. Zhong, R. Quhe, Z. Ni, M. Ye, W. N. Mei, J. Shi, W. Guo, J. Yang, and J. Lu, *Nanoscale* **7**, 2116–2127 (2015).
[28] J. Gong, Y. Tang, and P. Yang, *J. Mol. Struct.* 1064, 32–36 (2014).
[29] C. Sun and D. J. Searles, *J. Phys. Chem. C* **116**, 26222–26226 (2012).
[30] B. Jang, J. Koo, M. Park, H. Lee, J. Nam, and Y. Kwon, H. Lee, *Appl. Phys. Lett.* **103**, 263904 (2013).
[31] H. Zhang, Y. Xia, H. Bu, X. Wang, M. Zhang, Y. Luo, and M. Zhao, *J. Appl. Phys.* **113**, 044309 (2013).
[32] A. Mohajeri and A. Shahsavar, *Comput. Mater. Sci.* **115**, 51–59 (2016).
[33] Z. Xu, X. Lv, J. Li, J. Chen, and Q. Liu, *RSC Adv.* **6**, 25594–25600 (2016).
[34] Y. Jiao, A. Du, M. Hankel, Z. Zhu, V. Rudolph, and S. C. Smith, *Chem. Commun.* **47**, 11843–11845 (2011).
[35] S. W. Cranford and M. J. Buehler, *Nanoscale* **4**, 4587-4593 (2012).
[36] H. Zhang, X. He, M. Zhao, M. Zhang, L. Zhao, X. Feng, and Y. Luo, *J. Phys. Chem. C* **116**, 16634-16638 (2012).
[37] H. Zhang, X. Zhao, M. Zhang, Y. Luo, G. Li, and M. Zhao, *J. Phys. D: Appl. Phys.* **46**, 495307 (2013).
[38] M. Bartolomei, E. Carmona-Novillo, M. I. Hernández, J. Campos-Martínez, F. Pirani, and G. Giorgi, *J. Phys. Chem. C* **118**, 29966–29972 (2014).
[39] M. Bartolomei, E. Carmona-Novillo, M. I. Hernandez, J. Campos-Martinez, F. Pirani, G. Giorgi, and K. Yamashita, *J. Phys. Chem. Lett.* **5**, 751–755 (2014).
[40] Y. Jiao, A. Du, S. C. Smith, Z. Zhu, and S. Z. Qiao, *J. Mater. Chem. A* **3**, 6767–6771 (2015).
[41] X. Tan, L. Kou, H. A. Tahini, and S. C. Smith, *Mol. Simul.* **42**, 573–579 (2015).
[42] J. Kou, X. Zhou, Y. Chen, H. Lu, F. Wu, and J. Fan, *J. Chem. Phys.* **139**, 064705 (2013).
[43] M. Xue, H. Qiu, and W. Guo, *Nanotechnology* **24**, 505720 (2013).
[44] C. Zhu, H. Li, X. C. Zeng, E. G. Wang, and S. Meng, *Sci. Rep.* **3**, 3163 (2013).
[45] J. Kou, X. Zhou, H. Lu, F. Wu, and J. Fan, *Nanoscale* **6**, 1865-1870 (2014).
[46] Y. Liu, *Acta Chim. Sin.* **71**, 260 (2013).
[47] Z.-Z. Lin, *Carbon* **86**, 301–309 (2015).
[48] B. K. Das, D. Sen, and K. K. Chattopadhyay, *Phys. Chem. Chem. Phys.* **18**, 2949–2958 (2016).
[49] Z. Lu, S. Li, P. Lv, C. He, D. Ma, and Z. Yang, *Appl. Surf. Sci.* **360**, 1–7 (2016).
[50] X. Chen, P. Gao, L. Guo, and S. Zhang, *Sci Rep* **5**, 16720 (2015).
[51] Y. Zhang, L. Zhang, and C. Zhou, *Acc. Chem. Res.* **46**, 2329–2339 (2013).
[52] G. Binnig and H. Rohrer, *Rev. Mod. Phys.* **59**, 615–629 (1987).
[53] M. M. Haley, *Pure Appl. Chem.* **80**, 519–532 (2008).
[54] F. Diederich and M. Kivala, *Adv. Mater.* **22**, 803–812 (2010).
[55] F. Klappenberger, Y. Q. Zhang, J. Bjork, S. Klyatskaya, M. Ruben, and J. V. Barth, *Acc. Chem. Res.* **48**, 2140–2150 (2015).
[56] C. Glaser, *Berichte der deutschen chemischen Gesellschaft*, **2**, 422–424 (1869).
[57] I. D. Campbell and G. Eglinton, *Org. Synth.* **45**, 39 (1965).
[58] A. S. Hay, *J. Org. Chem.* **27**, 3320–3321 (1962).
[59] I. J. S. Fairlamb, P. S. Bäuerlein, L. R. Marrison, and J. M. Dickinson, *Chem. Commun.*, 632–633 (2003).
[60] Y. Q. Zhang, N. Kepcija, M. Kleinschrodt, K. Diller, S. Fischer, A. C. Papageorgiou, F. Allegretti, J. Bjork, S. Klyatskaya, F. Klappenberger, M. Ruben, and J. V. Barth, *Nat. Commun.* **3**, 1286 (2012).
[61] H. Y. Gao, H. Wagner, D. Zhong, J. H. Franke, A. Studer, and H. Fuchs, *Angew. Chem., Int. Ed.* **52**, 4024–4028 (2013).
[62] Q. Sun, L. Cai, H. Ma, C. Yuan, and W. Xu, *ACS Nano* **10**, 7023–7030 (2016).
[63] J. Björk, Y.-Q. Zhang, F. Klappenberger, J. V. Barth, and S. StafströmJ. *Phys. Chem. C* **18**, 3181–3187 (2014).
[64] a) B. Cirera, Y. Q. Zhang, J. Bjork, S. Klyatskaya, Z. Chen, M. Ruben, J. V. Barth, and F. Klappenberger, *Nano Lett.* **14**, 1891–1897 (2014). b) B. Cirera, Y. Q. Zhang, S. Klyatskaya, Ruben, F. Klappenberger, and J. V. Barth, *ChemCatChem* **5**, 3281–3288 (2013).
[65] J. Liu, Q. Chen, L. Xiao, J. Shang, X. Zhou, Y. Zhang, Y. Wang, X. Shao, J. Li, W. Chen, G. Q. Xu, H. Tang, D. Zhao, and K. Wu, *ACS Nano* **9**, 6305-6314 (2015).
[66] G. Fang and X. Bi, *Chem Soc. Rev.* **44**, 8124–8173 (2015).
[67] G.; Li, Y.; Li, H.; Liu, Y.; Guo, Y.; Li, and D. Zhu, *Chem. Commun.* **46**, 3256–3258 (2010).
[68] H. Liu, J. Xu, Y. Li, and Y. Li, *Acc. Chem. Res.* **43**, 1496–1508 (2010).
[69] J. Wang, S. Zhang, J. Zhou, R. Liu, R. Du, H. Xu, Z. Liu, J. Zhang, and Z. Liu, *Phys.Chem.Chem.Phys.* **16**, 11303–11309 (2014).

[70] A. C. Ferrari, J. C. Meyer, V. Scardaci, C. Casiraghi, M. Lazzeri, F. Mauri, S. Piscanec, D. Jiang, K. S. Novoselov, S. Roth, and A. K. Geim, *Phys. Rev. Lett.* **97**, 187401 (2006).

[71] L. J. Brillson, *Surf. Sci. Rep.* **2**, 123–326 (1982).

[72] X. Qian, H. Liu, C. Huang, S. Chen, L. Zhang, Y. Li, J. Wang, and Y. Li, *Sci. Rep.* **5**, 7756 (2015).

[73] M. Long, L. Tang, D. Wang, Y. Li, and Z. Shuai, *ACS Nano* **5**, 2593-2600 (2011).

[74] J. Zhou, X. Gao, R. Liu, Z. Xie, J. Yang, S. Zhang, G. Zhang, H. Liu, Y. Li, J. Zhang, and Z. Liu, *J. Am. Chem. Soc.* **137**, 7596-7599 (2015).

[75] G. Li, Y. Li, X. Qian, H. Liu, H. Lin, and N. Chen, Y. Li, *J. Phys. Chem. C* **115**, 2611–2615 (2011).

[76] Y. Li, L. Xu, H. Li, and Y. Li *Chem. Soc. Rev.*, **43**, 2572–2586 (2014). b) Q. Yue, S. Chang, J. Kang, S. Qin, and J. Li *J. Phys. Chem. C* **117** 14804–14811 (2013). c) J. Wang, A.-J. Zhang, and Y. Tang, *J. Appl. Phys.* **118**, 195102 (2015).

[77] M. M. Mahlambi, C. J. Ngila, and B. B. Mamba *J. Nanomaterials*, 790173 (2015).

[78] S. Wang, L. Yi, J. E. Halpert, X. Lai, Y. Liu, H. Cao, R. Yu, D. Wang, and Y. Li, *Small* **8**, 265–271 (2012).

[79] A. Karunya and H. Hsin-Yun *Molecules* **21**, 1585 (2016).b) Y. Yan, J. Miao, Z. Yang, F.-X. Xiao, H. B. Yang, B. Liu, and Y. Yang *Chem. Soc. Rev.* **44**, 3295–3346 (2015). c) A. Pandikumar, G. T. Soon How, T. P. See, F. S. Omar, S. Jayabal, K. Z. Kamali, N. Yuso, A. Jamil, R. Ramaraj, S. A. John, H. N. Lim, and N.M. Huang *RSC Adv.* **4**, 6329–63323 (2014).

[80] S. Thangavel, K. Krishnamoorthy, V. Krishnaswamy, N. Raju, S. J. Kim, and G. Venugopal, *J. Phys. Chem. C* **119**, 22057–22065 (2015).

[81] X. Zhang, M. Zhu, P. Chen, Y. Li, H. Liu, Y. Li, and M. Liu, *Phys. Chem. Chem. Phys.* **17**, 1217–1225 (2015).

[82] H. Qi, P. Yu, Y. Wang, G. Han, H. Liu, Y. Yi, Y. Li, and L. Mao, *J. Am. Chem. Soc.* **137**, 5260–5263 (2015).

[83] N. Yang, Y. Liu, H. Wen, Z. Tang, H. Zhao, Y. Li, and D. Wang, *ACS Nano* **7**, 1504–1512 (2013).

[84] H. C. Choi, M. Shim, S. Bangsaruntip, and H. Dai, *J. Am. Chem. Soc.* **124**, 9058-9 (2002).

[85] J. Li, X. Gao, B. Liu, Q. Feng, X. B. Li, M. Y. Huang, Z. Liu, J. C. Zhang, H. Tung, and L. Z. Wu, *J. Am. Chem. Soc.* **138**, 3954–3957 (2016).

[86] R. Liu, H. Liu, Y. Li, Y. Yi, X. Shang, S. Zhang, X. Yu, S. Zhang, H. Cao, and G. Zhang, *Nanoscale* **6**, 11336–11343 (2014).

[87] S. Zhang, Y. Cai, H. He, Y. Zhang, R. Liu, H. Cao, M. Wang, J. Liu, G. Zhang, Y. Li, H. Liu, and B. Li, *J. Mater. Chem. A* **4**, 4738-4744 (2016).

[88] I. Hijazi, T. Bourgeteau, R. Cornut, A. Morozan, A. Filoramo, J. Leroy, V. Derycke, B. Jousselme, and S. Campidelli, *J. Am. Chem. Soc.* **136**, 6348–6354 (2014).

[89] Y. Xue, Y. Guo, Y. Yi, Y. Li, H. Liu, D. Li, W. Yang, and Y. Li, *Nano Energy* **30**, 858–866 (2016). b) Y. Xue, J. Li, Z. Xue, Y. Li, H. Liu, D. Li, W. Yang, and Y. Li, *ACS Appl. Mater. Interfaces* **8**, 31083–31091 (2016).

[90] X. Gao, J. Zhou, R. Du, Z. Xie, S. Deng, R. Liu, Z. Liu, and J. Zhang, *Adv Mater* **28**, 168–173 (2016).

[91] C. Huang, S. Zhang, H. Liu, Y. Li, G. Cui, and Y. Li, *Nano Energy* **11**, 481–489 (2015).

[92] S. Zhang, H. Liu, C. Huang, G. Cui, and Y. Li, *Chem. Commun.* **51**, 1834–1837 (2015).

[93] S. Zhang, H. Du, J. He, C. Huang, H. Liu, and G. Cui, Y. Li, *ACS Appl. Mater. Interfaces*, **8**, 8467–8473 (2016).

[94] H. Du, H. Yang, C. Huang, J. He, H. Liu, and Y. Li, *Nano Energy* **22**, 615-622 (2016).

[95] K. Krishnamoorthy, S. Thangavel, J. Chelora Veetil, N. Raju, and G. Venugopal, and S. J. Kim, *Int. J. Hydrogen Energy* **41**, 1672–1678 (2016).

[96] H. Du, Z. Deng, Z. Lü, Y. Yin, L. Yu, H. Wu, Z. Chen, Y. Zou, Y. Wang, H. Liu, and Y. Li, *Synth. Met.* **161**, 2055–2057 (2011).

[97] Xiao, J., Shi, J., Liu, H., Xu, Y., Lv, S., Luo, Y., Li, D., Meng, Q., and Li, Y. *Advanced Energy Materials* **5**, 1401943 (2015).

[98] C. Kuang, G. Tang, T. Jiu, H. Yang, H. Liu, B. Li, W. Luo, X. Li, W. Zhang, F. Lu, and J. Fang, Y. Li, *Nano Lett.* **15**, 2756–2762 (2015).

[99] H. Ren, H. Shao, L. Zhang, D. Guo, Q. Jin, R. Yu, L. Wang, Y. Li, Y. Wang, H. Zhao, and D. Wang, *Adv. Energy Mater.* **5**, 1500296 (2015).

[100] C. Wang, P. Yu, S. Guo, L. Mao, H. Liu, and Y. Li, *Chem. Commun.* **52**, 5629–5632 (2016).

[101] K. Wu, J. Guo, and C. Wang, *Chem. Commun.* **50**, 695–697 (2014).